HHS Public Access

Author manuscript

Brain Behav Immun. Author manuscript; available in PMC 2024 October 01.

Published in final edited form as:

Brain Behav Immun. 2024 October ; 121: 365–383. doi:10.1016/j.bbi.2024.07.038.

House dust mite-induced asthma exacerbates Alzheimer's disease changes in the brain of the *App*$^{NL-G-F}$ mouse model of disease

Bijayani Sahu[a], **Suba Nookala**[a], **Angela M. Floden**[a], **Nilesh S. Ambhore**[b], **Venkatachalem Sathish**[b], **Marilyn G. Klug**[c], **Colin K. Combs**[a,*]

[a]Department of Biomedical Sciences, University of North Dakota, School of Medicine and Health Sciences, 1301 N Columbia Road, Grand Forks, ND 58202-9037, USA

[b]Department of Pharmaceutical Sciences, School of Pharmacy, College of Health and Human Sciences, North Dakota State University, Fargo, ND 58108-6050, USA

[c]Department of Population health, School of Medicine and Health Sciences, USA

Abstract

Alzheimer's disease (AD) is an age-related neurodegenerative disorder characterized by the accumulation of amyloid-β (Aβ) plaques, neuroinflammation, and neuronal death. Besides aging, various comorbidities increase the risk of AD, including obesity, diabetes, and allergic asthma. Epidemiological studies have reported a 2.17-fold higher risk of dementia in asthmatic patients. However, the molecular mechanism(s) underlying this asthma-associated AD exacerbation is unknown. This study was designed to explore house dust mite (HDM)-induced asthma effects on AD-related brain changes using the *App*$^{NL-G-F}$ transgenic mouse model of disease. Male and female 8–9 months old C57BL/6J wild type and *App*$^{NL-G-F}$ mice were exposed to no treatment, saline sham, or HDM extract every alternate day for 16 weeks for comparison across genotypes and treatment. Mice were euthanized at the end of the experiment, and broncho-alveolar lavage fluid (BALF), blood, lungs, and brains were collected. BALF was used to quantify immune cell phenotype, cytokine levels, total protein content, lactate dehydrogenase (LDH) activity, and total IgE. Lungs were sectioned and stained with hematoxylin and eosin, Alcian blue, and Masson's

*Corresponding author. colin.combs@und.edu (C.K. Combs).

CRediT authorship contribution statement

Bijayani Sahu: Writing – review & editing, Writing – original draft, Methodology, Investigation, Funding acquisition, Formal analysis, Data curation, Conceptualization. **SubaNookala:** Writing – review & editing, Writing – original draft, Methodology, Investigation, Formal analysis, Data curation. **Angela M. Floden:** Writing – review & editing, Project administration, Methodology. **Nilesh S. Ambhore:** Writing – review & editing, Writing – original draft, Methodology, Investigation, Formal analysis, Data curation. **Venkatachalem Sathish:** Writing – review & editing, Writing – original draft, Supervision, Methodology, Investigation, Funding acquisition, Formal analysis, Data curation. **Marilyn G. Klug:** Writing – review & editing, Methodology, Formal analysis. **Colin K. Combs:** Writing – review & editing, Writing – original draft, Supervision, Methodology, Investigation, Funding acquisition, Formal analysis, Data curation.

Declaration of Competing Interest

The authors declare that they have no known competing financial interests or personal relationships that could have appeared to influence the work reported in this paper.

Appendix A. Supplementary data

Supplementary data to this article can be found online at https://doi.org/10.1016/j.bbi.2024.07.038.

trichrome. Serum levels of cytokines and soluble Aβ1–40/42 were quantified. Brains were sectioned and immunostained for Aβ, GFAP, CD68, and collagen IV. Finally, frozen hippocampi and temporal cortices were used to perform Aβ ELISAs and cytokine arrays, respectively. HDM exposure led to increased levels of inflammatory cells, cytokines, total protein content, LDH activity, and total IgE in the BALF, as well as increased pulmonary mucus and collagen staining in both sexes and genotypes. Levels of serum cytokines increased in all HDM-exposed groups. Serum from the $App^{NL\text{-}G\text{-}F}$ HDM-induced asthma group also had significantly increased soluble Aβ1–42 levels in both sexes. In agreement with this peripheral change, hippocampi from asthma-induced male and female $App^{NL\text{-}G\text{-}F}$ mice demonstrated elevated Aβ plaque load and increased soluble Aβ 1–40/42 and insoluble Aβ 1–40 levels. HDM exposure also increased astrogliosis and microgliosis in both sexes of $App^{NL\text{-}G\text{-}F}$ mice, as indicated by GFAP and CD68 immunoreactivity, respectively. Additionally, HDM exposure elevated cortical levels of several cytokines in both sexes and genotypes. Finally, HDM-exposed groups also showed a disturbed blood–brain-barrier (BBB) integrity in the hippocampus of $App^{NL\text{-}G\text{-}F}$ mice, as indicated by decreased collagen IV immunoreactivity. HDM exposure was responsible for an asthma-like condition in the lungs that exacerbated Aβ pathology, astrogliosis, microgliosis, and cytokine changes in the brains of male and female $App^{NL\text{-}G\text{-}F}$ mice that correlated with reduced BBB integrity. Defining mechanisms of asthma effects on the brain may identify novel therapeutic targets for asthma and AD.

Keywords

Alzheimer’s disease; Asthma; Amyloid β; Neuroinflammation; Blood-Brain-Barrier

1. Introduction

Alzheimer’s disease (AD) is the most common age-related neurodegenerative disorder with long-term, life-threatening outcomes (Bondi et al., 2017; Breijyeh et al., 2020; Tiwari et al., 2019). The pathophysiology of AD includes extracellular amyloid beta (Aβ) plaque accumulation (Hardy and Selkoe, 2002), intracellular neurofibrillary tangles (Jia et al., 2005; Querfurth and LaFerla, 2010; Welge et al., 2009), gliosis, neuroinflammation, loss of synapses, and neuronal death, which eventually results in cognitive impairment (Kocahan and Dogan, 2017; Kumar et al., 2015; Ramirez-Bermudez, 2012).

The risks of developing AD are multifactorial, with aging being the most significant (Breijyeh and Karaman, 2020; Esiri and Chance, 2012; Uchoa et al., 2016). Aside from aging, environmental factors and comorbidities such as head trauma, obesity, diabetes, asthma, and air pollution also increase the risk of AD (Block and Calderon-Garciduenas, 2009; Calderon-Garciduenas et al., 2012; Uchoa et al., 2016). One possibility for these associations may be that peripheral immune changes communicate with the brain to influence the status of AD (Bettcher et al., 2021; Burgaletto et al., 2020; Cao and Zheng, 2018; Lutshumba et al., 2021; Rossi et al., 2021). For example, emerging evidence suggests a link between the occurrence of AD and asthma (Caldera-Alvarado et al., 2013; Chen et al., 2014; Joh et al., 2023; Kim et al., 2019; Nair et al., 2022; Ohrui et al., 2002; Peng et al., 2015). Several reports have also suggested that the prevalence of AD and asthma is significantly higher in the elderly (Bozek et al., 2016; Kim et al., 2019; Ng et al., 2007;

Ohrui et al., 2002; Wu et al., 2019). Epidemiological studies have reported a 2.17-fold increased risk of dementia in asthmatic patients over the age of 45 and a 1.27-fold increase in asthmatic patients under the age of 20 (Kim et al., 2019; Peng et al., 2015). These findings raise the possibility that chronic inflammatory diseases such as asthma may alter the progression of AD.

Asthma is characterized by persistent airway inflammation, bronchial hyperresponsiveness, and remodeling that affects approximately 25 million people in the United States (Dekkers et al., 2009; Kalidhindi et al., 2021; Lazaar and Panettieri, 2005; Murdoch and Lloyd, 2010; Prakash, 2013). It is distinguished by a classic set of symptoms including cough, wheeze, shortness of breath, variable airflow obstruction, and chest tightness, along with evidence of expiratory airflow limitation (Carpaij et al., 2019; Russell and Brightling, 2017). Moreover, chronic asthma may influence cognitive function during AD (Bozek and Jarzab, 2011; Heneka et al., 2015; Ishmael, 2011; Kim et al., 2019; Ohrui et al., 2002). To address a possible mechanistic connection between lung pathophysiology during asthma and AD-related brain changes, we investigated the effect of asthma on Aβ pathology, gliosis, inflammatory milieu, and blood–brain-barrier integrity using an HDM-induced mouse model of asthma in C57BL/6J wild type and $App^{NL\text{-}G\text{-}F}$ mice.

2. Materials and methods

2.1. Antibodies and reagents

For immunohistochemistry studies primary antibodies against glial fibrillary acidic protein (GFAP; D1F4Q) and amyloid beta (Aβ; D54D2) were purchased from Cell Signaling Technology, Inc. (Danvers, MA, USA). The CD68 (MCA1957) antibody was purchased from Bio-Rad Laboratories, Inc. (Hercules, CA, USA). The anti-collagen IV (ab236640) antibody was purchased from Abcam (Cambridge, MA, USA). Elite Vectastain ABC reagents, Vector VIP, biotinylated anti-rabbit, and anti-mouse secondary antibodies were purchased from Vector Laboratories, Inc (Burlingame, CA, USA).

2.2. Animal model

$App^{NL\text{-}G\text{-}F}$ mice were obtained from Dr. Takaomi C. Saido, Laboratory for Proteolytic Neuroscience, RIKEN Center for Brain Science, Japan. Amyloid precursor protein (APP) is not overexpressed in $App^{NL\text{-}G\text{-}F}$ mice, but pathogenic Aβ is elevated due to three mutations associated with familial AD. An APP construct containing a humanized Aβ region, which includes the Swedish “N”, the Iberian “F”, and the Arctic “G” mutations, was used to generate this mouse model (Saito et al., 2014). This model was selected to avoid potential artifacts introduced by APP overexpression. A total of 38 $App^{NL\text{-}G\text{-}F}$ (18 males and 20 females; n = 5–7/group) and 48 C57BL/6J wild type (WT) (24 males and 24 females; n = 7–9/group) littermate control mice were used at 8–9 months of age. The C57BL/6J mice were from an in-house colony originally obtained from Jackson Laboratories. All animal study protocols were approved by the Institutional Animal Care and Use Committee (IACUC) at the University of North Dakota. The animals were provided with food and water *ad libitum* and housed on a 12-h light/dark cycle.

2.3. House dust mite exposure

The calculated amount of HDM extract (833 μg/kg body weight), which included *Dermatophagoides farinae (Der f)* and *Dermatophagoides pteronysnus (Der p)* (Greer Laboratories, Lenoir, NC), was resuspended in sterile saline, and animals were exposed to aerosolized HDM by nebulization. The nebulizer exposure chamber was 5.4L capacity (12″ wide by 6″ high by 6″ deep). Animals were placed in the holding chamber housed in a biosafety cabinet and allowed to move freely while sterile saline (sham) or HDM was aerosol delivered via nebulizer through a connection tube into the holding chamber (HDM exposed group). This procedure was done every alternate day (Monday/Wednesday/Friday) three days a week for 16 weeks (Kanaya et al., 2022; Wang et al., 2023). All mice were treated during the same cohort and were euthanized 3–6 days after the last treatment of the 16 weeks of exposure. Control groups were not given any kind of treatment.

2.4. Broncho-alveolar lavage fluid (BALF) and tissue collections

At the end of the exposure period, animals were euthanized, and BALF, lungs, blood, and brains were collected. BALF was obtained by injecting 1 mL of ice-cold sterile Ca^{2+} and Mg^{2+}-free phosphate-buffered saline (PBS) into the lung and gently aspirating the fluid. The fluid recovery rate was more than 90 % (Sahu et al., 2018). The BALF was spun at 206 x *g* for 10 min at 4 °C, to obtain cell pellet, which was used for flow cytometric analysis. BALF supernatants were stored at −80 °C for subsequent analysis of cytokines, protein content, and lactate dehydrogenase (LDH) activity. Blood was used to separate serum for assessing cytokine and Aβ levels. Additionally, the left hemispheres of the brains and left lobes of the lungs were fixed in 4 % paraformaldehyde for immunohistochemical, hematoxylin and eosin (H&E), Alcian blue and Masson's trichrome staining. The right hemispheres were separated into hippocampus and cortical regions, then flash frozen in liquid nitrogen for ELISAs and cytokine analysis.

2.5. Phenotypic analysis of immune subsets in BALF by flow cytometry

BALF was collected in 1 mL of Ca^{2+} and Mg^{2+}-free PBS. The BALF was spun at 206 x *g* for 10 min at 4 °C, and the supernatant was transferred for further analysis. BALF cell pellets were resuspended in FACS buffer [Ca^{2+} and Mg^{2+}-free PBS supplemented with 2 % fetal bovine serum], used for immunophenotyping by multicolor flow cytometry (BD FACS Symphony A3). Red blood cells (RBCs) were lysed using RBC lysis buffer (eBioscience, ThermoFisher Scientific, CA, USA). Cells were resuspended in 150 μL of Live/Dead (Ghost dye 510, 1:1000; Tonbo Biosciences, CA, USA) prepared in PBS−/− without serum or proteins. The cells were incubated for 30 min at 4 °C, then spun down (297 x *g*, 4 °C, 10 min) and washed by adding 150 μL of FACS buffer to remove any unbound viability dye. The cells were resuspended in 150 μL of Fc Block (purified rat anti-mouse CD16/CD32, clone 2.4G2 (Biolegend, CA, USA) prepared 1: 50 dilution in FACS buffer and incubated for 10 min on ice (to prevent nonspecific binding of antibodies to Fc receptors). The cells were stained with an antibody cocktail that included BB515 labeled CD3 (Biolegend), PerCPCy5–5 labeled CD45 (Biolegend), Brilliant Violet (BV) 421 labeled Siglec-F (Biolegend), BV605 labeled CD4 (Biolegend), BV786 labeled CD19 (Biolegend), Phycoerythrin (PE) labeled – Ly6G (Biolegend), PECF594 labeled CD11c (Biolegend),

PECy5 labeled CD11b (Biolegend), PECy7 labeled CD68 (Biolegend), Allophycocyanin (APC)labeled Ly6C (Biolegend), APC-Cy7-labeled MHC-II (IA_IE) (Biolegend), Alexa Fluor 700 labeled NK1–1 (Biolegend). At least 10,000 events were collected on a BD FACS Symphony A3, and the data was analyzed using FlowJo™ v10.8.1 software (BD Life Sciences, Ashland, OR).

Selective surface markers were used for the definitive identification of T and B lymphocytes, neutrophils, dendritic cells, macrophages, eosinophils, and NK cells. Single stained, unstained, and fluorescence one minus controls were used to set compensation and manual gating, respectively (Germundson et al., 2022; Kaur et al., 2021). Plugins available in FlowJo software were used for checking signal and cleaning anomalies, clustering, and dimensionality reduction. Cells were initially gated on good events and cell debris, doublets, and non-viable cells were excluded (Germundson et al., 2022). Live cells expressing the pan leukocyte marker, $CD45^+$ were gated from singlets, and were subjected to further analysis of subsets. Dimensionality reduction of the flow cytometry data was performed using Uniform Manifold Approximation and Projection (UMAP) projection using the plugins in FlowJo software following default settings (Euclidean distance, nearest neighbors 15, minimum distance value 0.5, number of components 2) to visualize differences and spatial distribution of innate and adaptive immune populations. First,.fcs files from at least n = 3 mice per genotype per treatment condition were down sampled to 572 live events and concatenated. Manually gated populations were then overlaid on UMAP plots to get insights into the visual landscape of the dynamic changes in immune subsets and to uncover the most perturbed signatures following HDM exposure compared to sham and control groups among the genotypes. An unsupervised clustering algorithm, Self Organizing Map (FlowSOM), was employed using the default settings for clustering and identification of unique combinations of markers with similar levels of expression. Hierarchical clustering and column-scaled heatmaps were generated using Rstudio (v4.1.2). The gating strategy from a representative sample is shown in Suppl. Fig. 1. UMAP visualization helped with the identification of clusters and the existence of strong neighborhoods among immune subsets that would have been difficult to determine with manual gating (Suppl. Fig. 2).

2.6. Histopathology analysis using H&E, Alcian blue, and Masson’s trichrome staining

Paraffin-embedded lung tissues were cut into 6 μm sections using a rotary microtome (Leica, UK). The sections were stained with H&E to assess airway thickening and inflammatory cell recruitment, Alcian blue for examining mucous levels, and Masson’s trichrome stain to identify the extent of collagen deposition, using previously established techniques (Aich et al., 2012; Ambhore et al., 2019; Kalidhindi et al., 2021; Kalidhindi et al., 2019). The stained tissue sections were scanned at 20X using a Hamamatsu NanoZoomer 2.0-HT digital slide scanner. The scanned sections were processed in the NDP.view2Plus (Hamamatsu Photonics, Shizuoka, Japan) to capture the airway images. The average optical density (OD) of the airway thickening in the H&E stain, mucous levels in the Alcian blue stain, and collagen deposition in Masson’s trichrome stain were determined using ImageJ software (National Institutes of Health; https://rsb.info.nih.gov/ij).

2.7. Immunohistochemistry

The fixed left-brain hemisphere of each animal was processed for histologic studies as previously described (Nagamoto-Combs et al., 2016). After collection, brains were fixed in 4 % paraformaldehyde then cryoprotected in a gradient of 15 % sucrose-PBS and 30 % sucrose-PBS for 72 h each. The cryoprotected tissue was embedded in a 15 % gelatin-PBS matrix and was submerged in 4 % paraformaldehyde overnight, which enabled complete polymerization. Afterward, the gelatin brain blocks were cryoprotected by two changes of 30 % sucrose-PBS for 72 h. The blocks were then flash-frozen using dry ice and isopentane. Serial sections of 40 μm were cut using a Leica 2010R sliding microtome with a freezing stage (Physitemp, Clifton, NJ, USA) and stored at 4 °C in PBS with 0.1 % sodium azide until immunostaining. For collagen IV and Aβ, antigen retrieval was required. Collagen IV antigen retrieval was performed using pH 6.0 sodium citrate buffer at 95 °C for 10 min. For Aβ antigen retrieval, sections were incubated in 25 % formic acid for 25 min before blocking. No antigen retrieval was required for anti CD68. Sections were then incubated with primary anti-Aβ (1:500), anti-GFAP (1:1000), anti-CD68 (1:1000), and anti-collagen IV (1:2000) antibodies with mild shaking overnight at 4 °C. Primary antibody incubation was followed by washing and incubation with biotinylated secondary antibodies (1:2000) and an avidin/biotin complex (Vector ABC Elite kit). Vector VIP was used as the chromogen to visualize antibody binding. The sections were mounted onto gelatin subbed slides and cover-slipped using Permount (Fisher Scientific, Hampton, NH, USA)), with subsequent standard dehydration. As mentioned earlier, a Hamamatsu NanoZoomer 2.0-HT Brightfield + Fluorescence Slide Scanning System was used to capture images. The immunoreactivity quantitation was conducted using an open-source digitalized image analysis platform, QuPath (v.0.4.3) (Bankhead et al., 2017). The hippocampus regions of all brain sections were annotated using either the brush or the wand tool. Staining quantitation was performed as previously described (Morriss et al., 2020). For each tissue section, QuPath software grouped adjacent and similar pixels into a superpixel of 25 mm^2. Pixel similarity was determined by red–green–blue (RGB) values. After grouping into superpixels, QuPath software was used to apply an arbitrary intensity value for each superpixel to identify whether they were either positive or negative (Morriss et al., 2020; Sahu et al., 2023). The % positive superpixels calculated by Qupath were averaged and graphed as mean values ± SEM.

2.8. Enzyme-linked immunosorbent assay (ELISA)

Soluble and insoluble Aβ 1–40 and Aβ 1–42 ELISA.—The flash-frozen hippocampi were weighed and lysed in ice-cold RIPA buffer (20 mM Tris-HCl, pH 7.4, 150 mM NaCl, 1 mM Na_3VO_4, 10 mM NaF, 1 mM EDTA, 1 mM EGTA, 0.2 mM phenylmethylsulfonyl fluoride, 1 % Triton-X100, 0.1 % SDS, and 0.5 % deoxycholate) with protease inhibitors (1 mM AEBSF, 0.8 μM aprotinin, 21 μM leupeptin, 36 μM bestatin, 15 μM pepstatin A, 14 μME-64). The tissue samples were homogenized using Zirconium oxide beads (MidSci, MO, USA) in a Bullet Blender (Quasar instruments, CO, USA) and centrifuged to remove the insoluble content. The resulting supernatants were used to perform soluble Aβ 1–40 and Aβ 1–42 ELISAs. The protein concentrations of the sample lysates were measured using the bicinchoninic acid (BCA) protein determination assay (Thermo Fisher Scientific, MA, USA)

(Sahu et al., 2021). The insoluble content (pellet) was resuspended in 5 M guanidine HCl/50 mM Tris HCl pH 8.0, and samples were again homogenized using the Bullet Blender and centrifuged (21,000 g, 4 °C, 10 min), and the supernatants were used to perform insoluble Aβ 1–40 and Aβ 1–42 ELISAs. Serum samples were also collected for measuring Aβ 1–40/42 levels. The levels of soluble and insoluble Aβ 1–40 (EZBRAIN40) and Aβ 1–42 (EZBRAIN42) were assessed using commercially available ELISA kits (Millipore Sigma, Burlington, MA, USA). The levels of Aβ 1–40 and Aβ 1–42 (soluble and insoluble) were detected as pg/mL per mg protein derived from the standard curve for each protein.

Total IgE ELISA.—BALF supernatant was used to perform total IgE ELISA (EMIGHE) using a commercially available kit from Invitrogen (ThermoFisher Scientific, Waltham, MA, USA). BALF IgE levels were quantified using a standard curve and are presented in ng/mL.

2.9. Th1/Th2/Th17 cytokine assessment

RayBio Quantibody® Mouse TH17 Arrays (QAM-TH17–1, RayBio, Norcross, GA) were employed to assay BALF supernatant, serum, and temporal cortex lysates, following the manufacturer's instructions. Temporal cortex lysates were used for cytokine analysis as this is also a region with Aβ plaque and gliosis changes in $App^{NL\text{-}G\text{-}F}$ mice. Eighteen different cytokines were evaluated: IL-1β, IL-2, IL-4, IL-5, IL-6, IL-10, IL-12p70, IL-13, IL-17, IL-17F, IL-21, IL-22, IL-23, IL28, IFN-γ, MIP-3α, TGF-β, and TNF-α. RayBioTech used a GenePix 4400 scanner for scanning the slide arrays using GenePix Pro software. Results were analyzed using the RayBio Analysis Tool. Using a standard curve, concentrations of each cytokine were determined (pg/mL).

2.10. Statistical analysis

Results are presented as mean values ± standard error mean (SEM). Statistical analysis was performed by one-way and type III two-way ANOVAs. Significant interactions led to further analyses of subgroups. ANOVAs were followed by Tukey's multiple comparisons tests to control alpha inflation and increased Type I error using GraphPad Prism 10.1.2 software (GraphPad Software, Inc. La Jolla, CA) with $p < 0.05$ considered statistically significant. Male and female differences are compared relevant to their respective WT groups. Results are stratified by male and female and described according to these groups.

3. Results

3.1. HDM-exposed lungs had increased infiltration of inflammatory cells

BALF is an important resource for investigating cellular and humoral immune responses following allergen exposure and disease conditions. Changes in BALF immune subsets are predictive indicators of ongoing lung inflammation (Harbeck, 1998). To assess outcomes and changes to immune populations following HDM exposure, we investigated the immune changes in the BALF microenvironment in WT littermate and $App^{NL\text{-}G\text{-}F}$ mice using a two-way ANOVA between treatments and genotypes with Tukey's adjustment for multiple comparisons. The most robust changes were seen in HDM-exposed WT male mice compared to the other groups (Fig. 1A). Except for CD19 and Siglec-F (sialic acid binding immunoglobulin like lectin-F), HDM exposure induced significantly high levels of CD45,

CD3, CD3CD4 (CD4T), CD11b, CD11c, CD68, Ly6C, Ly6G, and NK1–1, compared to the control or sham groups (Fig. 1A, $p < 0.05$). However, CD3CD8T (CD8T) cell responses were significantly lower in the HDM-exposed WT male mice, thereby increasing the CD4/CD8 ratio ($p < 0.05$). Strikingly different HDM-induced responses were observed in male $App^{NL\text{-}G\text{-}F}$ mice, with significantly elevated levels of Ly6C, CD11c, NK1–1, CD11b, CD3, and Siglec-F expressing cells compared to the control or sham groups (Fig. 1A, $p < 0.05$). It is notable that while there was no significant induction of CD4T or CD8T cell response, the levels of Siglec-F produced by eosinophils and alveolar macrophages were significantly elevated in the HDM-exposed $App^{NL\text{-}G\text{-}F}$ male mice compared to the sham group (Fig. 1A, $p < 0.05$). When directly comparing the HDM-induced responses between WT and $App^{NL\text{-}G\text{-}F}$ males, it was clear that a cell-type selective blunted response was observed in $App^{NL\text{-}G\text{-}F}$ males with significantly reduced levels of CD11b, CD68, and Ly6G compared to WT mice (Fig. 1A, $p < 0.05$). The HDM-induced immune responses of WT female mice were similar to those seen in WT male mice except there were no significant differences in the levels of CD4T cells (Fig. 2A). Female $App^{NL\text{-}G\text{-}F}$ mice showed HDM-induced changes in the levels of CD45, CD3, CD11b, CD11c, Ly6C, and NK1- expressing cells when compared to sham or control groups (Fig. 2A, $p < 0.05$). Interestingly, when directly comparing the HDM exposure-induced changes between WT and $App^{NL\text{-}G\text{-}F}$ females, we again observed an attenuated response in the $App^{NL\text{-}G\text{-}F}$ mice with reduced CD45, CD11b, CD11c, CD68, IAIE, Ly6C, Ly6G, and NK1–1 levels compared to WT mice (Fig. 2A, $p < 0.05$).

While surface expression of several markers on NK cells has been characterized to affect distinct functional roles (Omi et al., 2014), our UMAP and clustering analysis showed that $Ly6C^{+}$ cells clustered with NK1–1 cells in the HDM-treated groups (Supp Fig. S2). Ly6C, a macrophage marker, is expressed on many cell types and elevated levels of Ly6C on CD4T cells is considered a useful marker in distinguishing memory and activated effector T cells. Data from our UMAP clustering further demonstrated that the CD11c expressing cells clustered with both CD4T and CD8T cells (Supp Fig. S2). HDM-induced CD11c expression was significantly upregulated in male and female WT and $App^{NL\text{-}G\text{-}F}$ male mice. Consistent with the increase in CD11c + cells, Th2 responses were more potent in HDM-exposed mice compared to Th1 responses (Supp Fig. S2). In agreement with the BALF findings, H&E evaluation of lung sections from the treatment groups demonstrated significantly increased airway thickening in HDM-exposed lungs from both sexes and genotypes compared to their respective sham and control groups (Suppl. Fig. S3, $p < 0.05$). Interestingly, in spite of the somewhat reduced cellular responses in $App^{NL\text{-}G\text{-}F}$ mice, both male and female $App^{NL\text{-}G\text{-}F}$ mice demonstrated significantly increased HDM-induced airway thickening compared to their respective WT group (Suppl. Fig. S3, $p < 0.05$).

3.2. HDM-exposed lungs demonstrated increased collagen and mucus production

The validity of the HDM model across genotypes was next assessed by evaluating mucus production and collagen deposition in lung sections via Alcian blue and Masson's trichrome staining, respectively. As expected, HDM exposure increased mucus staining (Fig. 3A) and collagen deposition (Fig. 3B) in male and female WT and $App^{NL\text{-}G\text{-}F}$ mice compared to their respective control and sham groups confirming the robustness of the HDM model ($p <$

0.05). Consistent with the H&E results (Suppl. Fig. S3), both sexes of $App^{NL\text{-}G\text{-}F}$ showed an HDM-associated elevation in mucus staining compared to their respective WT group (Fig. 3A, $p < 0.05$). HDM-exposed male $App^{NL\text{-}G\text{-}F}$ mice also showed an elevation in collagen staining compared to their WT counterparts (Fig. 3B, $p < 0.05$). Interestingly, both sexes of control $App^{NL\text{-}G\text{-}F}$ mice showed an increased level of mucus and collagen staining when compared to their respective WT group, indicating baseline AD-associated lung changes independent of HDM exposure.

3.3. Hdm-exposed lungs had elevated cytokine and total IgE levels

Inflammation is critical in regulating the pathophysiology and integrity of the airway in asthmatic lungs (Murdoch and Lloyd, 2010). To explore the pulmonary level of various cytokines, a slide-based RayBiotech Mouse Cytokine Array kit was used to assay BALF supernatant. With exposure to the HDM extract, significant elevations in the levels of TNF-α, IL-1β, IL-6, IFN-γ, IL-4, IL-5, and IL-13 were observed in both sexes of WT and $App^{NL\text{-}G\text{-}F}$ mice in comparison to the control or sham exposure groups (Figs. 4A & 5A, $p < 0.05$). Consistent with our findings of genotype selective changes in response to HDM exposure, both male and female $App^{NL\text{-}G\text{-}F}$ mice exhibited a reduced level of IL-1β and increased IL-4 compared to their respective WT group (Figs. 4A & 5A, $p < 0.05$). Additionally, female HDM-exposed $App^{NL\text{-}G\text{-}F}$ mice demonstrated a significant reduction in IL-L-6 and IL-13 levels, as well as a significant increase in IFN-γ and IL-4 levels compared to WT HDM-exposed mice (Fig. 5A, $p < 0.05$). These findings further support a unique pulmonary response to HDM exposure in the $App^{NL\text{-}G\text{-}F}$ mice.

In addition to cytokines, groups exposed to HDM exhibited significantly higher levels of total IgE in the BALF supernatant of both the sexes of WT and $App^{NL\text{-}G\text{-}F}$ mice in comparison to both the control and sham groups (Figs. 4D & 5D, $p < 0.05$). Interestingly, both sexes of $App^{NL\text{-}G\text{-}F}$ mice showed a significant elevation in BALF IgE levels, even in the control groups, in comparison to WT mice ($p < 0.05$), indicating distinct baseline lung differences between the genotypes as well as in response to HDM exposure.

3.4. HDM-exposed lungs had increased alveolar permeability

Increased alveolar-capillary membrane permeability across the endothelial and epithelial barriers, which results in pulmonary edema formation in the lungs, is another physiologic characteristic of asthmatic lungs (Dong et al., 2012). This change can be measured by the total protein content in the BALF supernatant. As shown in Figs. 4B & 5B, an increase in protein content was noted upon HDM exposure in BALF supernatant of both sexes of WT ($p < 0.05$). However, in $App^{NL\text{-}G\text{-}F}$ mice only female mice showed an increase in protein content upon HDM exposure when compared to control and sham exposure groups ($p < 0.05$), reflecting potent alveolar capillary leakage in the wild types and female $App^{NL\text{-}G\text{-}F}$ HDM-exposed animals. No genotype differences were observed between the WT and AD mice.

3.5. BALF supernatant from house dust mite-exposed lungs had increased LDH activity

Necrotic cell death is also associated with asthmatic lungs, leading to the loss of cell membrane integrity and the subsequent leakage of LDH into the extracellular spaces,

which may further attract inflammatory cells, adding to tissue damage (Drent et al., 1996). Therefore, LDH activity was assessed in the BALF supernatant as an indicator of cellular damage and death. Our data revealed that HDM exposure increased LDH activity in the BALF supernatant of both sexes of WT and $App^{NL\text{-}G\text{-}F}$ mice compared to control and sham exposure groups ($p < 0.05$). This data provided evidence of increased lung damage in the HDM-exposed groups (Figs. 4C & 5C). No genotype differences were observed between the WT and AD mice.

Based on these data, it was evident that chronic exposure to HDM exposure induced an asthma-like condition in the lungs of both genotypes, as suggested by the increased infiltration of inflammatory cells, increased cytokine levels, total BALF IgE levels, increased alveolar permeability, and lung tissue damage with uniquely different responses across genotype.

3.6. HDM-induced asthma increased systemic inflammation and soluble Aβ levels

Next, we determined the effect of HDM-induced asthma on systemic immune changes in the two genotypes. To assess circulating levels of various Th1/Th2 cytokines, serum cytokines were quantified. A significant elevation in TNF-α and IL-5 was observed in the HDM-induced asthma groups of both sexes of WT and $App^{NL\text{-}G\text{-}F}$ mice compared to control and sham exposure groups (Figs. 6A & 7A, $p < 0.05$). Both sexes of WT mice also showed a significant HDM-associated elevation in IFN-γ and IL-13 in comparison to the control and sham groups (Figs. 6A & 7A, $p < 0.05$). Female but not male $App^{NL\text{-}G\text{-}F}$ mice also demonstrated a significant elevation in the HDM-induced IL-13 levels compared to control and sham groups (Figs. 6A & 7A, $p < 0.05$). Additionally, once again $App^{NL\text{-}G\text{-}F}$ mice showed genotype selective differences in response to HDM exposure with reduced levels of IL-13 and IFN-γ in males and IL-3 and IL-5 in females compared to their WT counterparts (Figs. 6A & 7A, $p < 0.05$). Interestingly, in all comparison groups both male and female $App^{NL\text{-}G\text{-}F}$ mice had significantly increased levels of TNF-α and IL-6 compared to their respective WT groups once again supporting our observation of a subtle but genotype selective different in immune phenotype (Figs. 6A & 7A, $p < 0.05$).

We next asked whether HDM-induced asthma influenced the levels of Aβ in the serum of the $App^{NL\text{-}G\text{-}F}$ mice. The levels of both soluble Aβ 1–40 and Aβ 1–42 were measured from the serum of the male and female $App^{NL\text{-}G\text{-}F}$ mice by ELISA. Interestingly, only Aβ 1–42 levels were elevated in both sexes by HDM exposure compared to the control and sham groups (Figs. 6B & 7B, $p < 0.05$).

3.7. HDM-induced asthma increased Aβ accumulation in the hippocampus

Since brain Aβ plaque accumulation is one of the key pathological features of AD (Hardy and Selkoe, 2002) and increased circulating Aβ was observed (Figs. 6B & 7B), we next assessed whether HDM-induced asthma altered brain Aβ plaque load. Immunohistochemistry for Aβ was performed on the male and female $App^{NL\text{-}G\text{-}F}$ brains from the control, sham, and HDM-exposed groups. Similar to the serum changes, we observed a significant increase in Aβ plaque load in the hippocampus of the HDM-induced

asthma groups in comparison to both the control and the sham groups of both male and female $App^{NL\text{-}G\text{-}F}$ mice (Fig. 8A, $p < 0.05$).

As an additional means of quantitation, hippocampal Aβ levels were measured by ELISA assessing both Aβ 1–40 and Aβ 1–42. In parallel with the immunohistochemical data, soluble and insoluble Aβ 1–40 and soluble Aβ 1–42 levels were significantly elevated in both male and female $App^{NL\text{-}G\text{-}F}$ HDM-exposed mice compared to the control or sham brains (Fig. 8B, $p < 0.05$). There was no significant difference observed in the insoluble Aβ 1–42 levels among the groups (Fig. 8B).

3.8. HDM-induced asthma increased astrogliosis in the hippocampus of $App^{NL\text{-}G\text{-}F}$ mice

Astrocytes are the most abundant glial subtype in the CNS and play a crucial role in the regulation of neuroinflammation and are associated with the senile plaques in the brains of AD patients (Fakhoury, 2018). Therefore, to investigate the reactivity of astrocytes in response to HDM-induced asthma, brain sections were immunostained for GFAP. A basal level of hippocampal GFAP staining was detected in both sexes of WT mice, which was significantly increased by HDM-induced asthma in males but not females (Fig. 9, $p < 0.05$). On the other hand, HDM exposure increased hippocampal GFAP immunoreactivity in only female $App^{NL\text{-}G\text{-}F}$ and not male mice compared to the control and sham groups (Fig. 9, $p < 0.05$). Not surprisingly, both sexes of $App^{NL\text{-}G\text{-}F}$ mice showed significantly increased GFAP immunoreactivity in all treatment groups compared to their respective WT mice consistent with disease-associated astrogliosis (Fig. 9, $p < 0.05$).

3.9. HDM-induced asthma altered microglial phenotype in the hippocampus of $App^{NL\text{-}G\text{-}F}$ mice

Microglia are among the first cells activated and play a critical role in neuroinflammation associated with various neurodegenerative diseases, including AD (Fakhoury, 2018; Russell and Brightling, 2017). Microglial phenotype ranges from a resting state (with small extrusions), larger amoeboid microglia (with a reduced number of extrusions; rounded), to large, activated macrophage-like morphology (Hendrickx et al., 2017). CD68 expression can be a marker for a reactive, phagocytic phenotype of macrophages (Kurushima et al., 2000). Thus, to explore microglial activation in response to the HDM exposure, immunostaining of the brain sections for CD68 was performed. In WT mice, sporadic CD68 staining was observed in both sexes, which was not altered by HDM exposure (Fig. 10). Consistent with known disease-associated microgliosis, both sexes of $App^{NL\text{-}G\text{-}F}$ mice showed significantly increased CD68 immunoreactivity across all treatment groups compared to their respective WT group (Fig. 10, $p < 0.05$). It was intriguing to observe that HDM exposure significantly increased CD68 immunoreactivity in both sexes of $App^{NL\text{-}G\text{-}F}$ mice above sham and control group levels ($p < 0.05$). These data provide additional evidence that HDM-induced asthma can further potentiate microgliosis even above disease-induced levels (Fig. 10). This data demonstrated that asthma induced a microgliotic response preferentially in the brains of $App^{NL\text{-}G\text{-}F}$ and not WT mice.

3.10. HDM-induced asthma increased proinflammatory cytokine concentrations in the temporal cortex of App^{NL-G-F} mice

Based on the increased astrogliosis and microgliosis observed in the HDM-exposed brains, we expected that the inflammatory changes associated with the *App*$^{NL-G-F}$ brains would also be exacerbated. The levels of several pro and anti-inflammatory cytokines were assessed in the brains to test this idea using a slide-based cytokine array. In both WT and *App*$^{NL-G-F}$ male and female mice, TNF-α, IL-1β, IL-6, IFN-γ and IL-5 were elevated in the HDM-induced asthma groups compared to control and sham exposure groups (Figs. 11 & 12, $p < 0.05$). Additionally, the levels of IL-5 were significantly elevated in WT and *App*$^{NL-G-F}$ female HDM-induced asthma groups (Fig. 12, $p < 0.05$) while IL-13 showed a significant HDM-associated elevation in both sexes of *App*$^{NL-G-F}$ mice compared to controls (Figs. 11 & 12, $p < 0.05$). HDM exposure also significantly increased levels of IL-6 and IL-5 in both sexes of *App*$^{NL-G-F}$ compared to WT mice demonstrating once again a genotype selective response to exposure (Figs. 11 & 12, $p < 0.05$). Similarly, HDM-exposure significantly elevated levels of TNF-α, IL-1β, and IFN-γ in *App*$^{NL-G-F}$ females above WT mice (Fig. 11, $p < 0.05$). These data indicated that, similar to lungs, *App*$^{NL-G-F}$ mouse brains had a unique immune response to HDM-induced asthma compared to WT mice.

3.11. HDM-induced asthma altered BBB permeability in the hippocampus of App^{NL-G-F} mice

The BBB plays an important role in maintaining the homeostasis of the specialized microenvironment of the CNS, and disturbances in the BBB integrity have been implicated in many brain disorders, including AD (Almutairi et al., 2016). Therefore, to examine the effect of HDM-induced asthma on the BBB integrity, we assessed collagen IV immunoreactivity in the brains from WT and *App*$^{NL-G-F}$ mice in the control, sham, and HDM-induced asthma groups. Both sexes of *App*$^{NL-G-F}$ mice showed a significant decrease in collagen IV immunoreactivity across all groups when compared to WT mice consistent with disease-associated BBB compromise (Fig. 13, $p < 0.05$). No significant change in collagen IV immunoreactivity was observed in male or female WT mice suggesting a resistance to asthma-dependent vascular disruption (Fig. 13). On the other hand, HDM-induced asthma significantly reduced hippocampal collagen IV immunoreactivity in male and female *App*$^{NL-G-F}$ mice even beyond disease-associated levels when compared to control and sham groups (Fig. 13, $p < 0.05$). This data suggested that HDM-induced asthma disrupted the BBB integrity preferentially in the brains of the *App*$^{NL-G-F}$ mice.

4. Discussion

We investigated the effects of HDM-induced asthma on AD-associated brain changes. Our data suggest that chronic exposure to HDM extract induces an asthma-like condition in the lungs of both male and female WT and *App*$^{NL-G-F}$ mice. Surprisingly, there were subtle differences in the lungs basally and upon HDM exposure when comparing WT to *App*$^{NL-G-F}$ mice suggesting differences in peripheral immune cell behavior across genotypes that merit further study. Moreover, HDM-induced asthma communicated more robustly to the brains of the *App*$^{NL-G-F}$ compared to WT and exacerbated AD pathophysiology as evidenced by elevated Aβ plaque load and Aβ levels, increased astrogliosis and microgliosis, altered brain

inflammatory cytokine levels, and reduced BBB integrity. Our findings align with earlier research that has shown a relationship between the lungs and the brain (Li et al., 2023), as well as a reported exacerbation of AD pathology in asthma patients (Gan et al., 2022).

HDM exposure is a common environmental source of allergen and sensitivity is associated with greater than 80 % of asthmatics and disease severity (Gregory and Lloyd, 2011; Marks et al., 1995; Ruggieri et al., 2017). Additionally, sensitivities to particular species of dust mite are associated with more severe symptoms (Gao et al., 2023). Therefore, experimental mouse models of asthma increasingly rely on HDM exposure as a model of disease. Importantly, the HDM exposure model in mice is ideal since it is able to replicate airway inflammation and hyperreactivity, and most importantly, airway remodeling with collagen deposition (Johnson et al., 2004; Woo et al., 2018; Park et al., 2022). In humans, asthmatic severity is directly associated with airway remodeling and collagen deposition making the HDM exposure model ideal for use (Chetta et al., 1997; Tillie-Leblond et al., 2008). In our model, WT and $App^{NL\text{-}G\text{-}F}$ mice were exposed using an HDM nebulized delivery method. As mentioned, HDM is a major source of allergens responsible for the development of asthma (Miyamoto et al., 1970; Platts-Mills and Chapman, 1987). *Der f* and *Der p* are the most common species of HDM associated with the induction of asthma (Ishii et al., 2018; Yamashita et al., 1989). Therefore, extracts from these two species were selected for aerosolization to induce asthma in our study.

The pathophysiology of asthma includes the infiltration of inflammatory and allergy-specific cells, increased pulmonary cytokines, increased alveolar permeability, and lung injury (Peebles and Aronica, 2019). Our data revealed that the exposure to HDM extract for 16 weeks led to a pronounced infiltration of immune cells to the lungs, as indicated by the flow cytometry data from the BALF. As expected, the increased inflammatory reaction in the lungs led to increased alveolar permeability and injury to the lungs, as indicated by the increased protein content and LDH activity in the BALF supernatant. Although the H&E, Masson's trichrome, Alcian blue, BALF, and cytokine analyses from the HDM-exposed mice broadly demonstrated exposure-dependent changes, it was clear that there were significant differences when both sexes were compared to their respective genotype control and sham groups. Indeed, significant sex differences in the prevalence, severity, and immune responses associated with asthma has been reported (Shah and Newcomb, 2018). Females tend to have a higher prevalence and greater severity of asthma than males, and exhibit differences in lung function and airway inflammation (Shah and Newcomb, 2018). However, in the present study, HDM exposure induced a more robust immune cell infiltration into the lungs in the WT males. The $App^{NL\text{-}G\text{-}F}$ mice showed a similar, albeit attenuated, HDM-induced effect compared to WT mice among both sexes. It is important to consider that the differences in asthma and immune responses between genotypes are intricate and have multiple factors involved, both biological and environmental, that could affect them.

We also found that NK1–1^+ natural killer cells (NK cells) exhibited features of HDM responses that were common across all genotypes and, therefore, likely play an important role in chronic stimulation and production of inflammatory cytokines. While surface expression of several markers on NK cells has been characterized as affecting distinct

functional roles (Omi et al., 2014), increased NK cell activity has been reported to be associated with the promotion of allergic pulmonary inflammation (Kim and Jang, 2018) in the asthma condition in humans (Jira et al., 1988) and mice (Korsgren et al., 1999). Our cluster analysis also revealed the association of dendritic cells with the T cells, perhaps responsible for regulating the T cell activity. Several studies report that dendritic cells play a vital role in the regulation of airway inflammation and contribute to the pathogenesis of asthma by activating T cells (Gaurav and Agrawal, 2013; Morianos and Semitekolou, 2020). As mentioned, despite the overall similarity in the asthmatic phenotype induced by HDM exposure, there were unique immune-related changes that occurred in the $App^{NL\text{-}G\text{-}F}$ mice as indicated by reduced increases in several cytokines compared to WT mice. Indeed, using the ovalbumin model of allergic asthma others have reported similar findings of disparate immune responses in the lung when comparing WT mice to different AD lines (Sarlus et al., 2020; Wu et al., 2019). Future studies are needed to define disease-associated differences in particularly peripheral immune cell function in the $App^{NL\text{-}G\text{-}F}$ and other AD lines.

The roles of Th1 and Th2 cytokines in the pathogenesis of asthma have been extensively studied and it is known that the Th1 and Th2 cytokine balance plays an important role in allergic asthma (Truyen et al., 2006). The proinflammatory cytokines, especially TNF-α (Makwana et al., 2012), IL-1β (Dragon et al., 2007), IL-6 (Pedroza et al., 2011), and IFN-γ (Raundhal et al., 2015) are known for regulating airway inflammation, hyperresponsiveness, and remodeling, while the Th2 cytokines, IL-4, IL-5, and IL-13 regulate the development and pathogenesis of asthma (Barnes, 2001). Pulmonary secretory cytokines levels, including the Th1 and Th2 categories, were elevated in our study, indicative of an increased inflammatory and allergy-like condition, respectively. In addition to the pulmonary levels, serum concentrations of a few Th1 cytokines, such as TNF-α and IFN-γ, and Th2 cytokines, IL-5 and IL-13, were also elevated in our study which is in parallel with prior reports (Agache et al., 2016; Cembrzynska-Nowak et al., 1993; Dimitrova et al., 2019). Additionally, the Th1 cytokines and IL-5 from Th2 cytokines also showed a significant elevation in HDM-exposed brains of $App^{NL\text{-}G\text{-}F}$ mice. Although IL-5 levels correlate with AD severity (Wood et al., 2015), its essential role in AD pathology is yet to determined. Since IL-5 is neurotrophic and known to promote progenitor differentiation into neurons (Mehler et al., 1993), its upregulation could be an attempt to compensate for neuronal dysfunction in the $App^{NL\text{-}G\text{-}F}$ brain. A study by Lewkowich et al. also reported that repeated exposure to HDM results in altered neuroimmune status (Lewkowich et al., 2020) supporting our observations of overall lung-to-brain communication. It is unclear whether the elevated brain cytokines we observed in the $App^{NL\text{-}G\text{-}F}$ brains were due to increased local production or influx via increased permeability of the BBB as suggested by our data of reduced vascular integrity in the $App^{NL\text{-}G\text{-}F}$ mice during the HDM-induced asthma condition.

Overall, our findings support an altered and perhaps blunted response in the $App^{NL\text{-}G\text{-}F}$ asthmatic phenotype compared to the littermate C57BL/6 wild type mice. This finding is consistent with other reports. Using an ovalbumin-induced asthma model in the APP/PS1 amyloidosis model of AD, prior work has shown that there is an attenuated asthma response in the APP/PS1 line compared to C57BL/6J mice. The APP/PS1 mice had a significantly lower level of asthma-induced airway hypertension and changes in lung compliance compared to the C57BL/6J mice (Wu et al., 2019). This correlated with a

lower level of eosinophils in the BALF of the asthma-induced APP/PS1 mice compared to asthma-induced C57BL/6 wild type mice (Wu et al., 2019). As a possible explanation for this blunted response in the APP/PS1 line, the authors identified an increase in lung Foxp3+/CD4 + T regulatory cells with correspondingly reduced Foxp3 promoter and CpG region methylation in the asthma-induced APP/PS1 mice compared to the asthma-induced C57BL/6 mice (Wu et al., 2019). Although both our mouse and asthma model differ in the current study, it is possible that APP or its proteolytic products, such as Aβ, influence T cell phenotype. For example, it has been demonstrated that CD4 + and CD8 + T cells express APP and its expression is increased with mitogenic stimulation and it is proteolyzed for secretion (Monning et al., 1992; Monning et al., 1990). It is clear that there are additional targets for γ-secretase besides APP in lymphoid organs (Laky et al., 2009), but inhibition of γ-secretase with the inhibitor, LY-411,575 impairs lymphocyte development (Wong et al., 2004). In addition, *in vitro* stimulation with APP proteolytic products is sufficient to increase lymphocyte proliferation (Trieb et al., 1996). Finally, *in vivo* stimulation with intraperitoneal injected Aβ 1–42 peptide, using an experimental autoimmune encephalomyelitis (EAE) C57BL/6 mouse model of multiple sclerosis, was able to reduce clinical symptoms and numbers of CD4 + Th17 T cells (Shi et al., 2022). Further work is necessary to determine the roles of wild type and mutant APP and their proteolytic fragments on regulating particularly T cell phenotype. Increasing knowledge in this area will be useful for improving a broad understanding of the biology of this protein and its contribution to immune cell behavior. Effort in this area will also have direct relevance to AD since it is clear that brain and amyloid-specific T cells influence brain presentation of disease (Browne et al., 2013; Dansokho et al., 2016; Machhi et al., 2021; McQuillan et al., 2010; Spani et al., 2015; Yeapuri et al., 2023).

Since the main aim of our work was to explore the effect of HDM exposure on AD-related brain changes, we examined the accumulation of amyloid plaques in the brain, one of the major pathological hallmarks of AD (Hardy and Selkoe, 2002). Interestingly, our data demonstrated that amyloid-associated pathology was enhanced with chronic exposure to HDM in both sexes of $App^{NL\text{-}G\text{-}F}$ mice. The increase in plaque load was further confirmed by significantly elevated levels of soluble Aβ 1–40/42 and insoluble Aβ 1–40 in the hippocampus. Interestingly, soluble levels of Aβ1–42 levels were found to also be elevated in the serum of the $App^{NL\text{-}G\text{-}F}$ HDM-induced asthma groups. According to a report by Bu et al., chronic peripheral inflammatory stress may contribute to an increase in soluble Aβ proteins in serum (Bu et al., 2015). Many studies also suggest that there exists a dynamic balance between the Aβ levels in the brain and in the circulation (Bu et al., 2015; Ghersi-Egea et al., 1996; Roberts et al., 2014). It has been demonstrated in both humans and animal models that Aβ is transported from the brain into the circulations under particular conditions (Ghersi-Egea et al., 1996; Roberts et al., 2014). Therefore, the higher serum Aβ levels may signify a greater Aβ burden in the brain. On the other hand, other reports suggest that Aβ from the periphery can also enter the brain and exacerbate the development of AD (Eisele et al., 2010; Sutcliffe et al., 2011). Moreover, elevated Aβ levels in serum could reduce its clearance from the brain (Marques et al., 2009). In addition, it has been reported that serum Aβ levels might also stem from peripheral organs expressing APP and its proteolytic enzymes (Nalivaeva and Turner, 2013). For instance, serum Aβ is reported to be increased

as a response to hypoxia associated with lung dysfunction in patients with COPD (Bu et al., 2015). Therefore, it is currently unclear whether the origin of elevated serum Aβ in the HDM-induced asthma mice is due to the efflux of amyloid protein from the brain, production of the protein by peripheral organs, or a combination of both. The impaired BBB evidenced by reduced vascular integrity might contribute to altered transport of Aβ to and from the brain. Further studies are required to determine the cause and sources for elevations of both brain and serum Aβ levels during the HDM-induced asthmatic response.

Normal BBB integrity is critical for protecting the brain from systemic toxins and maintaining CNS homeostasis and the necessary levels of nutrients and ions for neuronal function (Almutairi et al., 2016). The breakdown of the BBB in AD is hypothesized to contribute to the accumulation of insoluble extracellular plaques of Aβ along the walls of blood vessels, causing inflammation in the neurovascular unit (Kang et al., 2017). Moreover, pathological markers of AD are also associated with BBB impairment, which results in microglial activation, neuroinflammation, neurodegeneration, and cognitive impairment (Iadecola, 2017). BBB breakdown or impairment is associated with AD (Montagne et al., 2015). Our data showed a significant reduction in the levels of collagen IV in AD mice which was further reduced by the HDM-induced asthmatic condition, suggesting potentiation of BBB compromise beyond the levels already induced by disease. Disturbances in BBB permeability and structure may be caused directly by proinflammatory factors TNF-α, IFN-γ, and IL-1β (Daneman and Prat, 2015; Gloor et al., 2001; Gosselin and Rivest, 2007; Rivest et al., 2000; Zhuang et al., 2012) or indirectly through other mediators like MMP-9 (Nguyen et al., 2006; Wong et al., 2007). Some studies have shown that immune mediators, either through the circulation or via the olfactory nerve, infiltrate the brain, leading to neuroinflammation and gliosis (Block and Calderon-Garciduenas, 2009; Block et al., 2012). This correlates with our data of increased serum proinflammatory cytokine levels, TNF-α and IFN-γ, in all HDM-induced asthma groups. Surprisingly, despite the similar cytokine changes in the WT HDM-induced asthmatic brains, they did not demonstrate impairment in the BBB. The $App^{NL\text{-}G\text{-}F}$ mice appear to have a basally impaired vascular compartment that confers selective vulnerability to the changes induced by the asthmatic condition. Future efforts to fully characterize vascular function across sex and genotype as well as the sources for asthma-induced vascular change are necessary.

Our findings demonstrate that chronic exposure to house dust mite extract is sufficient to induce an asthma-like condition in the lungs of $App^{NL\text{-}G\text{-}F}$ mice in a similar fashion in both males and females. With the exception of some cytokine level changes, we observed that WT mice brains are resistant to changes induced by our HDM exposure model. It is important to note, however, that humans with asthma typically undergo chronic HDM exposure on a time scale much longer than the 16 weeks of our paradigm. In addition, the response of WT mice in the brain may not be resistant to asthma-induced change, per se, but may instead proceed along a different trajectory than the $App^{NL\text{-}G\text{-}F}$ mice that ultimately leads to the same or an even greater magnitude of effect. HDM exposure produced numerous significant brain changes in both sexes of $App^{NL\text{-}G\text{-}F}$ mice. This may suggest that asthma is capable of communicating to the brain to potentiate AD-related changes as an exacerbation of an existing brain phenotype. Moreover, it is feasible that a primed lung-to-brain communication pathway exists due to underlying AD-related mechanisms in

the $App^{NL\text{-}G\text{-}F}$ mice such as vascular compromise or basal levels of gliosis. Although it is not yet clear what molecules or cells are responsible for the HDM-induced exacerbation of AD brain phenotype, it is possible that asthma can communicate dysfunction to the brain beyond the paradigm of AD and could apply to other chronic neurodegenerative conditions (Cheng et al., 2015; Hill et al., 2019; Kwon et al., 2023; Manouchehrinia et al., 2015). This study provides compelling and novel insight toward improving our understanding of why asthma serves as a positive risk factor for Alzheimer's disease.

Supplementary Material

Refer to Web version on PubMed Central for supplementary material.

Acknowledgments

The authors thank Dr. Sathiya Priya Chandrasekaran, Dr. Takako Takaku, Dr. Santhosh Mukundan, Dr. Abhijit Satpati, and Natalia Frolov for their technical support.

Funding

This work was supported by funding from AARF-21-850265, RF1AG083029, and R01AG057046. Histological and flow cytometry services were provided by the UND Histology Core Facility and the North Dakota Flow Cytometry and Cell Sorting Core (NDFCCS) at UND, respectively. Both were supported by the NIH/NIGMS award P20GM113123, DaCCoTA CTR NIH grant U54GM128729, and UND SMHS funds.

Data availability

Data will be made available on request.

References

Agache I, Strasser DS, Klenk A, Agache C, Farine H, Ciobanu C, Groenen PM, Akdis CA, 2016. Serum IL-5 and IL-13 consistently serve as the best predictors for the blood eosinophilia phenotype in adult asthmatics. Allergy 71, 1192–1202. [PubMed: 27060452]

Aich J, Mabalirajan U, Ahmad T, Agrawal A, Ghosh B, 2012. Loss-of-function of inositol polyphosphate-4-phosphatase reversibly increases the severity of allergic airway inflammation. Nat. Commun 3, 877. [PubMed: 22673904]

Almutairi MM, Gong C, Xu YG, Chang Y, Shi H, 2016. Factors controlling permeability of the blood-brain barrier. Cell. Mol. Life Sci 73, 57–77. [PubMed: 26403789]

Ambhore NS, Kalidhindi RSR, Loganathan J, Sathish V, 2019. Role of Differential Estrogen Receptor Activation in Airway Hyperreactivity and Remodeling in a Murine Model of Asthma. Am. J. Respir. Cell Mol. Biol 61, 469–480. [PubMed: 30958966]

Bankhead P, Loughrey MB, Fernandez JA, Dombrowski Y, McArt DG, Dunne PD, McQuaid S, Gray RT, Murray LJ, Coleman HG, James JA, Salto-Tellez M, Hamilton PW, 2017. QuPath: Open source software for digital pathology image analysis. Sci. Rep 7, 16878. [PubMed: 29203879]

Barnes PJ, 2001. Th2 cytokines and asthma: an introduction. Respir. Res 2, 1–2. [PubMed: 11686858]

Bettcher BM, Tansey MG, Dorothee G, Heneka MT, 2021. Publisher Correction: Peripheral and central immune system crosstalk in Alzheimer disease - a research prospectus. Nat. Rev. Neurol 17, 724. [PubMed: 34625724]

Block ML, Calderon-Garciduenas L, 2009. Air pollution: mechanisms of neuroinflammation and CNS disease. Trends Neurosci. 32, 506–516. [PubMed: 19716187]

Block ML, Elder A, Auten RL, Bilbo SD, Chen H, Chen JC, Cory-Slechta DA, Costa D, Diaz-Sanchez D, Dorman DC, Gold DR, Gray K, Jeng HA, Kaufman JD, Kleinman MT, Kirshner A, Lawler C, Miller DS, Nadadur SS, Ritz B, Semmens EO, Tonelli LH, Veronesi B, Wright RO, Wright

RJ, 2012. The outdoor air pollution and brain health workshop. Neurotoxicology 33, 972–984. [PubMed: 22981845]

Bondi MW, Edmonds EC, Salmon DP, 2017. Alzheimer's Disease: Past, Present, and Future. J. Int. Neuropsychol. Soc 23, 818–831. [PubMed: 29198280]

Bozek A, Bednarski P, Jarzab J, 2016. Allergic rhinitis, bronchial asthma and other allergies in patients with Alzheimer's disease: unnoticed issue. Postepy Dermatol Alergol 33, 353–358. [PubMed: 27881942]

Bozek A, Jarzab J, 2011. Improved activity and mental function related to proper antiasthmatic treatment in elderly patients with Alzheimer's disease. Allergy Asthma Proc. 32, 341–345. [PubMed: 22195685]

Breijyeh Z, Karaman R, Review, C., on Alzheimer's Disease: Causes and Treatment,, 2020. Molecules 25.

Browne TC, McQuillan K, McManus RM, O'Reilly JA, Mills KH, Lynch MA, 2013. IFN-gamma Production by amyloid beta-specific Th1 cells promotes microglial activation and increases plaque burden in a mouse model of Alzheimer's disease. J. Immunol 190, 2241–2251. [PubMed: 23365075]

Bu XL, Cao GQ, Shen LL, Xiang Y, Jiao SS, Liu YH, Zhu C, Zeng F, Wang QH, Wang YR, He Y, Zhou HD, Wang YJ, 2015. Serum Amyloid-Beta Levels are Increased in Patients with Chronic Obstructive Pulmonary Disease. Neurotox. Res 28, 346–351. [PubMed: 26243505]

Burgaletto C, Munafo A, Di Benedetto G, De Francisci C, Caraci F, Di Mauro R, Bucolo C, Bernardini R, Cantarella G, 2020. The immune system on the TRAIL of Alzheimer's disease. J. Neuroinflammation 17, 298. [PubMed: 33050925]

Caldera-Alvarado G, Khan DA, Defina LF, Pieper A, Brown ES, 2013. Relationship between asthma and cognition: the Cooper Center Longitudinal Study. Allergy 68, 545–548. [PubMed: 23409872]

Calderon-Garciduenas L, Kavanaugh M, Block M, D'Angiulli A, Delgado-Chavez R, Torres-Jardon R, Gonzalez-Maciel A, Reynoso-Robles R, Osnaya N, Villarreal-Calderon R, Guo R, Hua Z, Zhu H, Perry G, Diaz P, 2012. Neuroinflammation, hyperphosphorylated tau, diffuse amyloid plaques, and down-regulation of the cellular prion protein in air pollution exposed children and young adults. J. Alzheimers Dis 28, 93–107. [PubMed: 21955814]

Cao W, Zheng H, 2018. Peripheral immune system in aging and Alzheimer's disease. Mol. Neurodegener 13, 51. [PubMed: 30285785]

Carpaij OA, Burgess JK, Kerstjens HAM, Nawijn MC, van den Berge M, 2019. A review on the pathophysiology of asthma remission. Pharmacol. Ther 201, 8–24. [PubMed: 31075356]

Cembrzynska-Nowak M, Szklarz E, Inglot AD, Teodorczyk-Injeyan JA, 1993. Elevated release of tumor necrosis factor-alpha and interferon-gamma by bronchoalveolar leukocytes from patients with bronchial asthma. Am. Rev. Respir. Dis 147, 291–295. [PubMed: 8430950]

Chen MH, Li CT, Tsai CF, Lin WC, Chang WH, Chen TJ, Pan TL, Su TP, Bai YM, 2014. Risk of dementia among patients with asthma: a nationwide longitudinal study. J. Am. Med. Dir. Assoc 15, 763–767. [PubMed: 25037169]

Cheng CM, Wu YH, Tsai SJ, Bai YM, Hsu JW, Huang KL, Su TP, Li CT, Tsai CF, Yang AC, Lin WC, Pan TL, Chang WH, Chen TJ, Chen MH, 2015. Risk of developing Parkinson's disease among patients with asthma: a nationwide longitudinal study. Allergy 70, 1605–1612. [PubMed: 26310430]

Chetta A, Foresi A, Del Donno M, Bertorelli G, Pesci A, Olivieri D, 1997. Airways remodeling is a distinctive feature of asthma and is related to severity of disease. Chest 111, 852–857. [PubMed: 9106559]

Daneman R, Prat A, 2015. The blood-brain barrier. Cold Spring Harb. Perspect. Biol 7, a020412.

Dansokho C, Ait Ahmed D, Aid S, Toly-Ndour C, Chaigneau T, Calle V, Cagnard N, Holzenberger M, Piaggio E, Aucouturier P, Dorothee G, 2016. Regulatory T cells delay disease progression in Alzheimer-like pathology. Brain 139, 1237–1251. [PubMed: 26912648]

Dekkers BG, Maarsingh H, Meurs H, Gosens R, 2009. Airway structural components drive airway smooth muscle remodeling in asthma. Proc. Am. Thorac. Soc 6, 683–692. [PubMed: 20008876]

Dimitrova D, Youroukova V, Ivanova-Todorova E, Tumangelova-Yuzeir K, Velikova T, 2019. Serum levels of IL-5, IL-6, IL-8, IL-13 and IL-17A in pre-defined groups of adult patients with moderate and severe bronchial asthma. Respir. Med 154, 144–154. [PubMed: 31260861]

Dong C, Wang G, Li B, Xiao K, Ma Z, Huang H, Wang X, Bai C, 2012. Antiasthmatic agents alleviate pulmonary edema by upregulating AQP1 and AQP5 expression in the lungs of mice with OVA-induced asthma. Respir. Physiol. Neurobiol 181, 21–28. [PubMed: 22226856]

Dragon S, Rahman MS, Yang J, Unruh H, Halayko AJ, Gounni AS, 2007. IL-17 enhances IL-1β-mediated CXCL-8 release from human airway smooth muscle cells. American Journal of Physiology-Lung Cellular and Molecular Physiology 292, L1023–L1029. [PubMed: 17189320]

Drent M, Cobben NA, Henderson RF, Wouters EF, van Dieijen-Visser M, 1996. Usefulness of lactate dehydrogenase and its isoenzymes as indicators of lung damage or inflammation. Eur. Respir. J 9, 1736–1742. [PubMed: 8866602]

Eisele YS, Obermüller U, Heilbronner G, Baumann F, Kaeser SA, Wolburg H, Walker LC, Staufenbiel M, Heikenwalder M, Jucker M, 2010. Peripherally applied Aβ-containing inoculates induce cerebral β-amyloidosis. Science 330, 980–982. [PubMed: 20966215]

Esiri MM, Chance SA, 2012. Cognitive reserve, cortical plasticity and resistance to Alzheimer's disease. Alzheimers Res. Ther 4, 7. [PubMed: 22380508]

Fakhoury M, 2018. Microglia and Astrocytes in Alzheimer's Disease: Implications for Therapy. Curr. Neuropharmacol 16, 508–518. [PubMed: 28730967]

Gan W, Kang M, Lv C, Zhao Z, Wu Y, Zhang X, Wang R, 2022. Asthma Aggravates Alzheimer's Disease by Up-Regulating NF-B Signaling Pathway Through LTD4. Available at SSRN 4033977.

Gao Y, Li J, Xu X, Wang C, Zhang Y, Zhang L, 2023. Sensitisation to House Dust Mite Component Der p 23 Is Associated with Severe Symptoms and Asthma in Allergic Rhinitis Patients. Int. Arch. Allergy Immunol 184, 906–913. [PubMed: 37437556]

Gaurav R, Agrawal DK, 2013. Clinical view on the importance of dendritic cells in asthma. Expert Rev. Clin. Immunol 9, 899–919. [PubMed: 24128155]

Germundson DL, Nookala S, Smith NA, Warda Y, Nagamoto-Combs K, 2022. HLA-II Alleles Influence Physical and Behavioral Responses to a Whey Allergen in a Transgenic Mouse Model of Cow's Milk Allergy. Front Allergy 3, 870513.

Ghersi-Egea JF, Gorevic P, Ghiso J, Frangione B, Patlak C, Fenstermacher J, 1996. Fate of cerebrospinal fluid-borne amyloid β-peptide: rapid clearance into blood and appreciable accumulation by cerebral arteries. J. Neurochem 67, 880–883. [PubMed: 8764620]

Gloor SM, Wachtel M, Bolliger MF, Ishihara H, Landmann R, Frei K, 2001. Molecular and cellular permeability control at the blood-brain barrier. Brain Res. Brain Res. Rev 36, 258–264. [PubMed: 11690623]

Gosselin D, Rivest S, 2007. Role of IL-1 and TNF in the brain: twenty years of progress on a Dr. Jekyll/Mr. Hyde duality of the innate immune system. Brain Behav. Immun 21, 281–289. [PubMed: 17275255]

Gregory LG, Lloyd CM, 2011. Orchestrating house dust mite-associated allergy in the lung. Trends Immunol. 32, 402–411. [PubMed: 21783420]

Harbeck RJ, 1998. Immunophenotyping of bronchoalveolar lavage lymphocytes. Clin. Diagn. Lab. Immunol 5, 271–277. [PubMed: 9605975]

Hardy J, Selkoe DJ, 2002. The amyloid hypothesis of Alzheimer's disease: progress and problems on the road to therapeutics. Science 297, 353–356. [PubMed: 12130773]

Hendrickx DAE, van Eden CG, Schuurman KG, Hamann J, Huitinga I, 2017. Staining of HLA-DR, Iba1 and CD68 in human microglia reveals partially overlapping expression depending on cellular morphology and pathology. J. Neuroimmunol 309, 12–22. [PubMed: 28601280]

Heneka MT, Carson MJ, El Khoury J, Landreth GE, Brosseron F, Feinstein DL, Jacobs AH, Wyss-Coray T, Vitorica J, Ransohoff RM, Herrup K, Frautschy SA, Finsen B, Brown GC, Verkhratsky A, Yamanaka K, Koistinaho J, Latz E, Halle A, Petzold GC, Town T, Morgan D, Shinohara ML, Perry VH, Holmes C, Bazan NG, Brooks DJ, Hunot S, Joseph B, Deigendesch N, Garaschuk O, Boddeke E, Dinarello CA, Breitner JC, Cole GM, Golenbock DT, Kummer MP, 2015. Neuroinflammation in Alzheimer's disease. Lancet Neurol. 14, 388–405. [PubMed: 25792098]

Hill E, Abboud H, Briggs FBS, 2019. Prevalence of asthma in multiple sclerosis: A United States population-based study. Mult. Scler. Relat. Disord 28, 69–74. [PubMed: 30557818]

Iadecola C, 2017. The Neurovascular Unit Coming of Age: A Journey through Neurovascular Coupling in Health and Disease. Neuron 96, 17–42. [PubMed: 28957666]

Ishii T, Niikura Y, Kurata K, Muroi M, Tanamoto K, Nagase T, Sakaguchi M, Yamashita N, 2018. Time-dependent distinct roles of Toll-like receptor 4 in a house dust mite-induced asthma mouse model. Scand. J. Immunol 87.

Ishmael FT, 2011. The inflammatory response in the pathogenesis of asthma. J. Am. Osteopath. Assoc 111, S11–S17.

Jia JP, Meng R, Sun YX, Sun WJ, Ji XM, Jia LF, 2005. Cerebrospinal fluid tau, Abeta1–42 and inflammatory cytokines in patients with Alzheimer's disease and vascular dementia. Neurosci. Lett 383, 12–16. [PubMed: 15936505]

Jira M, Antosova E, Vondra V, Strejcek J, Mazakova H, Prazakova J, 1988. Natural killer and interleukin-2 induced cytotoxicity in asthmatics. I. Effect of Acute Antigen-Specific Challenge. Allergy 43, 294–298. [PubMed: 2455455]

Joh H-K, Kwon H, Son KY, Yun JM, Cho SH, Han K, Park J-H, Cho B, 2023. Allergic diseases and risk of incident dementia and Alzheimer's Disease. Ann. Neurol 93, 384–397. [PubMed: 36093572]

Johnson JR, Wiley RE, Fattouh R, Swirski FK, Gajewska BU, Coyle AJ, Gutierrez-Ramos JC, Ellis R, Inman MD, Jordana M, 2004. Continuous exposure to house dust mite elicits chronic airway inflammation and structural remodeling. Am. J. Respir. Crit. Care Med 169, 378–385. [PubMed: 14597485]

Kalidhindi RSR, Ambhore NS, Bhallamudi S, Loganathan J, Sathish V, 2019. Role of Estrogen Receptors alpha and beta in a Murine Model of Asthma: Exacerbated Airway Hyperresponsiveness and Remodeling in ERbeta Knockout Mice. Front. Pharmacol 10, 1499. [PubMed: 32116656]

Kalidhindi RSR, Ambhore NS, Balraj P, Schmidt T, Khan MN, Sathish V, 2021. Androgen receptor activation alleviates airway hyperresponsiveness, inflammation, and remodeling in a murine model of asthma. Am. J. Physiol. Lung Cell. Mol. Physiol 320, L803–L818. [PubMed: 33719566]

Kanaya A, Yang M, Emala C, Mikami M, 2022. Chronic allergic lung inflammation negatively influences neurobehavioral outcomes in mice. J. Neuroinflammation 19, 210. [PubMed: 36045388]

Kang S, Lee YH, Lee JE, 2017. Metabolism-Centric Overview of the Pathogenesis of Alzheimer's Disease. Yonsei Med. J 58, 479–488. [PubMed: 28332351]

Kaur H, Nookala S, Singh S, Mukundan S, Nagamoto-Combs K, Combs CK, 2021. Sex-Dependent Effects of Intestinal Microbiome Manipulation in a Mouse Model of Alzheimer's Disease. Cells 10.

Kim JH, Jang YJ, 2018. Role of Natural Killer Cells in Airway Inflammation. Allergy, Asthma Immunol. Res 10, 448–456. [PubMed: 30088365]

Kim SY, Min C, Oh DJ, Choi HG, 2019. Risk of neurodegenerative dementia in asthma patients: a nested case-control study using a national sample cohort. BMJ Open 9, e030227.

Kocahan S, Dogan Z, 2017. Mechanisms of Alzheimer's Disease Pathogenesis and Prevention: The Brain, Neural Pathology, N-methyl-D-aspartate Receptors, Tau Protein and Other Risk Factors. Clin. Psychopharmacol. Neurosci 15, 1–8. [PubMed: 28138104]

Korsgren M, Persson CG, Sundler F, Bjerke T, Hansson T, Chambers BJ, Hong S, Van Kaer L, Ljunggren HG, Korsgren O, 1999. Natural killer cells determine development of allergen-induced eosinophilic airway inflammation in mice. J. Exp. Med 189, 553–562. [PubMed: 9927517]

Kumar A, Singh A, Ekavali,, 2015. A review on Alzheimer's disease pathophysiology and its management: an update. Pharmacol. Rep 67, 195–203. [PubMed: 25712639]

Kurushima H, Ramprasad M, Kondratenko N, Foster DM, Quehenberger O, Steinberg D, 2000. Surface expression and rapid internalization of macrosialin (mouse CD68) on elicited mouse peritoneal macrophages. J. Leukoc. Biol 67, 104–108. [PubMed: 10648004]

Kwon MJ, Kim JH, Kang HS, Lim H, Kim MJ, Kim NY, Kim SH, Choi HG, Kim ES, 2023. Possible Incidental Parkinson's Disease following Asthma: A Nested Case-Control Study in Korea. J Pers Med 13.

Laky K, Annaert W, Fowlkes BJ, 2009. Amyloid precursor family proteins are expressed by thymic and lymph node stromal cells but are not required for lymphocyte development. Int. Immunol 21, 1163–1174. [PubMed: 19710207]

Lazaar AL, Panettieri RA Jr., 2005. Airway smooth muscle: a modulator of airway remodeling in asthma. J. Allergy Clin. Immunol 116, 488–495 quiz 496. [PubMed: 16159613]

Lewkowich I, Ahlbrand R, Johnson E, McAlees J, Nawreen N, Raman R, Lingel I, Hargis J, Hoover C, Sah R, 2020. Modulation of fear behavior and neuroimmune alterations in house dust mite exposed A/J mice, a model of severe asthma. Brain Behav. Immun 88, 688–698. [PubMed: 32380274]

Li C, Chen W, Lin F, Li W, Wang P, Liao G, Zhang L, 2023. Functional Two-Way Crosstalk Between Brain and Lung: The Brain-Lung Axis. Cell. Mol. Neurobiol 43, 991–1003. [PubMed: 35678887]

Lutshumba J, Nikolajczyk BS, Bachstetter AD, 2021. Dysregulation of Systemic Immunity in Aging and Dementia. Front. Cell. Neurosci 15, 652111.

Machhi J, Yeapuri P, Lu Y, Foster E, Chikhale R, Herskovitz J, Namminga KL, Olson KE, Abdelmoaty MM, Gao J, Quadros RM, Kiyota T, Jingjing L, Kevadiya BD, Wang X, Liu Y, Poluektova LY, Gurumurthy CB, Mosley RL, Gendelman HE, 2021. CD4+ effector T cells accelerate Alzheimer's disease in mice. J. Neuroinflammation 18, 272. [PubMed: 34798897]

Makwana R, Gozzard N, Spina D, Page C, 2012. TNF-alpha-induces airway hyperresponsiveness to cholinergic stimulation in guinea pig airways. Br. J. Pharmacol 165, 1978–1991. [PubMed: 21951209]

Manouchehrinia A, Edwards LJ, Roshanisefat H, Tench CR, Constantinescu CS, 2015. Multiple sclerosis course and clinical outcomes in patients with comorbid asthma: a survey study. BMJ Open 5, e007806.

Marks GB, Tovey ER, Green W, Shearer M, Salome CM, Woolcock AJ, 1995. The effect of changes in house dust mite allergen exposure on the severity of asthma. Clin Exp Allergy 25, 114–118. [PubMed: 7750002]

Marques MA, Kulstad JJ, Savard CE, Green PS, Lee SP, Craft S, Watson G, Cook DG, 2009. Peripheral amyloid-β levels regulate amyloid-β clearance from the central nervous system. J. Alzheimers Dis 16, 325–329. [PubMed: 19221422]

McQuillan K, Lynch MA, Mills KH, 2010. Activation of mixed glia by Abeta-specific Th1 and Th17 cells and its regulation by Th2 cells. Brain Behav. Immun 24, 598–607. [PubMed: 20060887]

Mehler MF, Rozental R, Dougherty M, Spray DC, Kessler JA, 1993. Cytokine regulation of neuronal differentiation of hippocampal progenitor cells. Nature 362, 62–65. [PubMed: 8383296]

Miyamoto T, Oshima S, Domae A, Takahashi K, Izeki M, 1970. Allergenic potency of different house dusts in relation to contained mites. Ann. Allergy 28, 405–412. [PubMed: 5521172]

Monning U, Konig G, Prior R, Mechler H, Schreiter-Gasser U, Masters CL, Beyreuther K, 1990. Synthesis and secretion of Alzheimer amyloid beta A4 precursor protein by stimulated human peripheral blood leucocytes. FEBS Lett. 277, 261–266. [PubMed: 2125277]

Monning U, Konig G, Banati RB, Mechler H, Czech C, Gehrmann J, Schreiter-Gasser U, Masters CL, Beyreuther K, 1992. Alzheimer beta A4-amyloid protein precursor in immunocompetent cells. J. Biol. Chem 267, 23950–23956. [PubMed: 1429732]

Montagne A, Barnes SR, Sweeney MD, Halliday MR, Sagare AP, Zhao Z, Toga AW, Jacobs RE, Liu CY, Amezcua L, Harrington MG, Chui HC, Law M, Zlokovic BV, 2015. Blood-brain barrier breakdown in the aging human hippocampus. Neuron 85, 296–302. [PubMed: 25611508]

Morianos I, Semitekolou M, 2020. Dendritic Cells: Critical Regulators of Allergic Asthma. Int. J. Mol. Sci 21.

Morriss NJ, Conley GM, Ospina SM, Meehan Iii WP, Qiu J, Mannix R, 2020. Automated Quantification of Immunohistochemical Staining of Large Animal Brain Tissue Using QuPath Software. Neuroscience 429, 235–244. [PubMed: 31982467]

Murdoch JR, Lloyd CM, 2010. Chronic inflammation and asthma. Mutat. Res 690, 24–39. [PubMed: 19769993]

Nagamoto-Combs K, Manocha GD, Puig K, Combs CK, 2016. An improved approach to align and embed multiple brain samples in a gelatin-based matrix for simultaneous histological processing. J. Neurosci. Methods 261, 155–160. [PubMed: 26743972]

Nair AK, Hulle CAV, Bendlin BB, Zetterberg H, Blennow J, Wild N, Kollmorgen G, Suridjan I, Busse WW, Rosenkranz MA, 2022. Asthma amplifies dementia risk: evidence from CSF biomarkers and cognitive decline. Alzheimers Dement (NY) 8, e12315.

Nalivaeva NN, Turner AJ, 2013. The amyloid precursor protein: a biochemical enigma in brain development, function and disease. FEBS Lett. 587, 2046–2054. [PubMed: 23684647]

Ng TP, Chiam PC, Kua EH, 2007. Mental disorders and asthma in the elderly: a population-based study. Int. J. Geriatr. Psychiatry 22, 668–674. [PubMed: 17154223]

Nguyen JH, Yamamoto S, Steers J, Sevlever D, Lin W, Shimojima N, Castanedes-Casey M, Genco P, Golde T, Richelson E, Dickson D, McKinney M, Eckman CB, 2006. Matrix metalloproteinase-9 contributes to brain extravasation and edema in fulminant hepatic failure mice. J. Hepatol 44, 1105–1114. [PubMed: 16458990]

Ohrui T, Arai H, Ichinose M, Matsui T, Yamaya M, Sasaki H, 2002. Relationship between asthma severity and progression of Alzheimer's disease. Thorax 57, 561.

Omi A, Enomoto Y, Kiniwa T, Miyata N, Miyajima A, 2014. Mature resting Ly6C (high) natural killer cells can be reactivated by IL-15. Eur. J. Immunol 44, 2638–2647. [PubMed: 24995967]

Park S-Y, Kang M-J, Jin N, Lee SY, Lee YY, Jo S, Eom JY, Han H, Chung SI, Jang K, Kim T-H, Park J, Han J-S, 2022. House dust mite-induced Akt-ERK1/2-C/EBP beta pathway triggers CCL20-mediated inflammation and epithelial–mesenchymal transition for airway remodeling. FASEB J. 36, e22452.

Pedroza M, Schneider DJ, Karmouty-Quintana H, Coote J, Shaw S, Corrigan R, Molina JG, Alcorn JL, Galas D, Gelinas R, Blackburn MR, 2011. Interleukin-6 contributes to inflammation and remodeling in a model of adenosine mediated lung injury. PLoS One 6, e22667.

Peebles RS Jr., Aronica MA, 2019. Proinflammatory Pathways in the Pathogenesis of Asthma. Clin. Chest Med 40, 29–50. [PubMed: 30691715]

Peng YH, Wu BR, Su CH, Liao WC, Muo CH, Hsia TC, Kao CH, 2015. Adult asthma increases dementia risk: a nationwide cohort study. J. Epidemiol. Community Health 69, 123–128. [PubMed: 25271249]

Platts-Mills TA, Chapman MD, 1987. Dust mites: immunology, allergic disease, and environmental control. J. Allergy Clin. Immunol 80, 755–775. [PubMed: 3320157]

Prakash YS, 2013. Airway smooth muscle in airway reactivity and remodeling: what have we learned? Am. J. Physiol. Lung Cell. Mol. Physiol 305, L912–L933. [PubMed: 24142517]

Querfurth HW, LaFerla FM, 2010. Alzheimer's disease. N. Engl. J. Med 362, 329–344. [PubMed: 20107219]

Ramirez-Bermudez J, 2012. Alzheimer's disease: critical notes on the history of a medical concept. Arch. Med. Res 43, 595–599. [PubMed: 23178566]

Raundhal M, Morse C, Khare A, Oriss TB, Milosevic J, Trudeau J, Huff R, Pilewski J, Holguin F, Kolls J, Wenzel S, Ray P, Ray A, 2015. High IFN-gamma and low SLPI mark severe asthma in mice and humans. J. Clin. Invest 125, 3037–3050. [PubMed: 26121748]

Rivest S, Lacroix S, Vallieres L, Nadeau S, Zhang J, Laflamme N, 2000. How the blood talks to the brain parenchyma and the paraventricular nucleus of the hypothalamus during systemic inflammatory and infectious stimuli. Proc. Soc. Exp. Biol. Med 223, 22–38. [PubMed: 10632958]

Roberts KF, Elbert DL, Kasten TP, Patterson BW, Sigurdson WC, Connors RE, Ovod V, Munsell LY, Mawuenyega KG, Miller-Thomas MM, 2014. Amyloid-β efflux from the central nervous system into the plasma. Ann. Neurol 76, 837–844. [PubMed: 25205593]

Rossi B, Santos-Lima B, Terrabuio E, Zenaro E, Constantin G, 2021. Common Peripheral Immunity Mechanisms in Multiple Sclerosis and Alzheimer's Disease. Front. Immunol 12, 639369.

Ruggieri S, Drago G, Longo V, Colombo P, Balzan M, Bilocca D, Zammit C, Montefort S, Scaccianoce G, Cuttitta G, Viegi G, Cibella F, Group RP, 2017. Sensitization to dust mite defines different phenotypes of asthma: A multicenter study. Pediatr. Allergy Immunol 28, 675–682. [PubMed: 28783215]

Russell RJ, Brightling C, 2017. Pathogenesis of asthma: implications for precision medicine. Clin. Sci. (Lond.) 131, 1723–1735. [PubMed: 28667070]

Sahu B, Johnson LM, Sohrabi M, Usatii AA, Craig RMJ, Kaelberer JB, Chandrasekaran SP, Kaur H, Nookala S, Combs CK, 2023. Effects of Probiotics on Colitis-Induced Exacerbation of Alzheimer's Disease in $App^{NL\text{-}G\text{-}F}$ Mice. Int J Mol Sci 24.

Sahu B, Sandhir R, Naura AS, 2018. Two hit induced acute lung injury impairs cognitive function in mice: A potential model to study cross talk between lung and brain. Brain Behav. Immun 73, 633–642. [PubMed: 30026058]

Sahu B, Mackos AR, Floden AM, Wold LE, Combs CK, 2021. Particulate Matter Exposure Exacerbates Amyloid-beta Plaque Deposition and Gliosis in APP/PS1 Mice. J. Alzheimers Dis 80, 761–774. [PubMed: 33554902]

Saito T, Matsuba Y, Mihira N, Takano J, Nilsson P, Itohara S, Iwata N, Saido TC, 2014. Single App knock-in mouse models of Alzheimer's disease. Nat. Neurosci 17, 661–663. [PubMed: 24728269]

Sarlus H, Codita A, Wang X, Cedazo-Minguez A, Schultzberg M, Oprica M, 2020. Chronic airway allergy induces pro-inflammatory responses in the brain of wildtype mice but not 3xTg AD mice. Neuroscience 448, 14–27. [PubMed: 32916195]

Shah R, Newcomb DC, 2018. Sex bias in asthma prevalence and pathogenesis. Front. Immunol 9, 2997. [PubMed: 30619350]

Shi C, Cha J, Gong J, Wang S, Zeng P, Lian J, Zhang B, Hua Q, Lv J, Du C, Xie X, Zhang R, 2022. Amelioration of Experimental Autoimmune Encephalomyelitis in Alzheimer's Disease Mouse Models: A Potential Role for Abeta. Cells 11.

Spani C, Suter T, Derungs R, Ferretti MT, Welt T, Wirth F, Gericke C, Nitsch RM, Kulic L, 2015. Reduced beta-amyloid pathology in an APP transgenic mouse model of Alzheimer's disease lacking functional B and T cells. Acta Neuropathol. Commun 3, 71. [PubMed: 26558367]

Sutcliffe JG, Hedlund PB, Thomas EA, Bloom FE, Hilbush BS, 2011. Peripheral reduction of β-amyloid is sufficient to reduce brain β-amyloid: Implications for Alzheimer's disease. J. Neurosci. Res 89, 808–814. [PubMed: 21374699]

Tillie-Leblond I, de Blic J, Jaubert F, Wallaert B, Scheinmann P, Gosset P, 2008. Airway remodeling is correlated with obstruction in children with severe asthma. Allergy 63, 533–541. [PubMed: 18394127]

Tiwari S, Atluri V, Kaushik A, Yndart A, Nair M, 2019. Alzheimer's disease: pathogenesis, diagnostics, and therapeutics. Int. J. Nanomed 14, 5541–5554.

Trieb K, Ransmayr G, Sgonc R, Lassmann H, Grubeck-Loebenstein B, 1996. APP peptides stimulate lymphocyte proliferation in normals, but not in patients with Alzheimer's disease. Neurobiol. Aging 17, 541–547. [PubMed: 8832628]

Truyen E, Coteur L, Dilissen E, Overbergh L, Dupont LJ, Ceuppens JL, Bullens DM, 2006. Evaluation of airway inflammation by quantitative Th1/Th2 cytokine mRNA measurement in sputum of asthma patients. Thorax 61, 202–208. [PubMed: 16449261]

Uchoa MF, Moser VA, Pike CJ, 2016. Interactions between inflammation, sex steroids, and Alzheimer's disease risk factors. Front. Neuroendocrinol 43, 60–82. [PubMed: 27651175]

Wang D, Li W, Albasha N, Griffin L, Chang H, Amaya L, Ganguly S, Zeng L, Keum B, Gonzalez-Navájas JM, Levin M, AkhavanAghdam Z, Snyder H, Schwartz D, Tao A, Boosherhri LM, Hoffman HM, Rose M, Estrada MV, Varki N, Herdman S, Corr M, Webster NJG, Raz E, Bertin S, 2023. Longterm exposure to house dust mites accelerates lung cancer development in mice. J. Exp. Clin. Cancer Res 42, 26. [PubMed: 36670473]

Welge V, Fiege O, Lewczuk P, Mollenhauer B, Esselmann H, Klafki HW, Wolf S, Trenkwalder C, Otto M, Kornhuber J, Wiltfang J, Bibl M, 2009. Combined CSF tau, p-tau181 and amyloid-beta 38/40/42 for diagnosing Alzheimer's disease. J. Neural Transm. (Vienna) 116, 203–212. [PubMed: 19142572]

Wong GT, Manfra D, Poulet FM, Zhang Q, Josien H, Bara T, Engstrom L, Pinzon-Ortiz M, Fine JS, Lee HJ, Zhang L, Higgins GA, Parker EM, 2004. Chronic treatment with the gamma-secretase inhibitor LY-411,575 inhibits beta-amyloid peptide production and alters lymphopoiesis and intestinal cell differentiation. J. Biol. Chem 279, 12876–12882. [PubMed: 14709552]

Wong D, Prameya R, Dorovini-Zis K, 2007. Adhesion and migration of polymorphonuclear leukocytes across human brain microvessel endothelial cells are differentially regulated by endothelial cell

adhesion molecules and modulate monolayer permeability. J. Neuroimmunol 184, 136–148. [PubMed: 17291598]

Woo LN, Guo WY, Wang X, Young A, Salehi S, Hin A, Zhang Y, Scott JA, Chow CW, 2018. A 4-Week Model of House Dust Mite (HDM) Induced Allergic Airways Inflammation with Airway Remodeling. Sci. Rep 8, 6925. [PubMed: 29720689]

Wood LB, Winslow AR, Proctor EA, McGuone D, Mordes DA, Frosch MP, Hyman BT, Lauffenburger DA, Haigis KM, 2015. Identification of neurotoxic cytokines by profiling Alzheimer's disease tissues and neuron culture viability screening. Sci. Rep 5, 16622. [PubMed: 26564777]

Wu Y, Zhao Y, Xu T, You L, Zhang H, Liu F, 2019. Alzheimer's Disease Affects Severity of Asthma Through Methylation Control of Foxp3 Promoter. J. Alzheimers Dis 70, 121–129. [PubMed: 31127789]

Yamashita N, Haida M, Suko M, Okudaira H, Miyamoto T, 1989. Allergens of the house dust mite Dermatophagoides farinae. II. Immunological characterization of four allergenic molecules. Int. Arch. Allergy Appl. Immunol 88, 173–175. [PubMed: 2496039]

Yeapuri P, Machhi J, Lu Y, Abdelmoaty MM, Kadry R, Patel M, Bhattarai S, Lu E, Namminga KL, Olson KE, Foster EG, Mosley RL, Gendelman HE, 2023. Amyloid-beta specific regulatory T cells attenuate Alzheimer's disease pathobiology in APP/PS1 mice. Mol. Neurodegener 18, 97. [PubMed: 38111016]

Zhuang L, Liu X, Xu X, Yue C, Shu H, Bai F, Yu H, Shi Y, Zhang Z, 2012. Association of the interleukin 1 beta gene and brain spontaneous activity in amnestic mild cognitive impairment. J. Neuroinflammation 9, 263. [PubMed: 23199001]

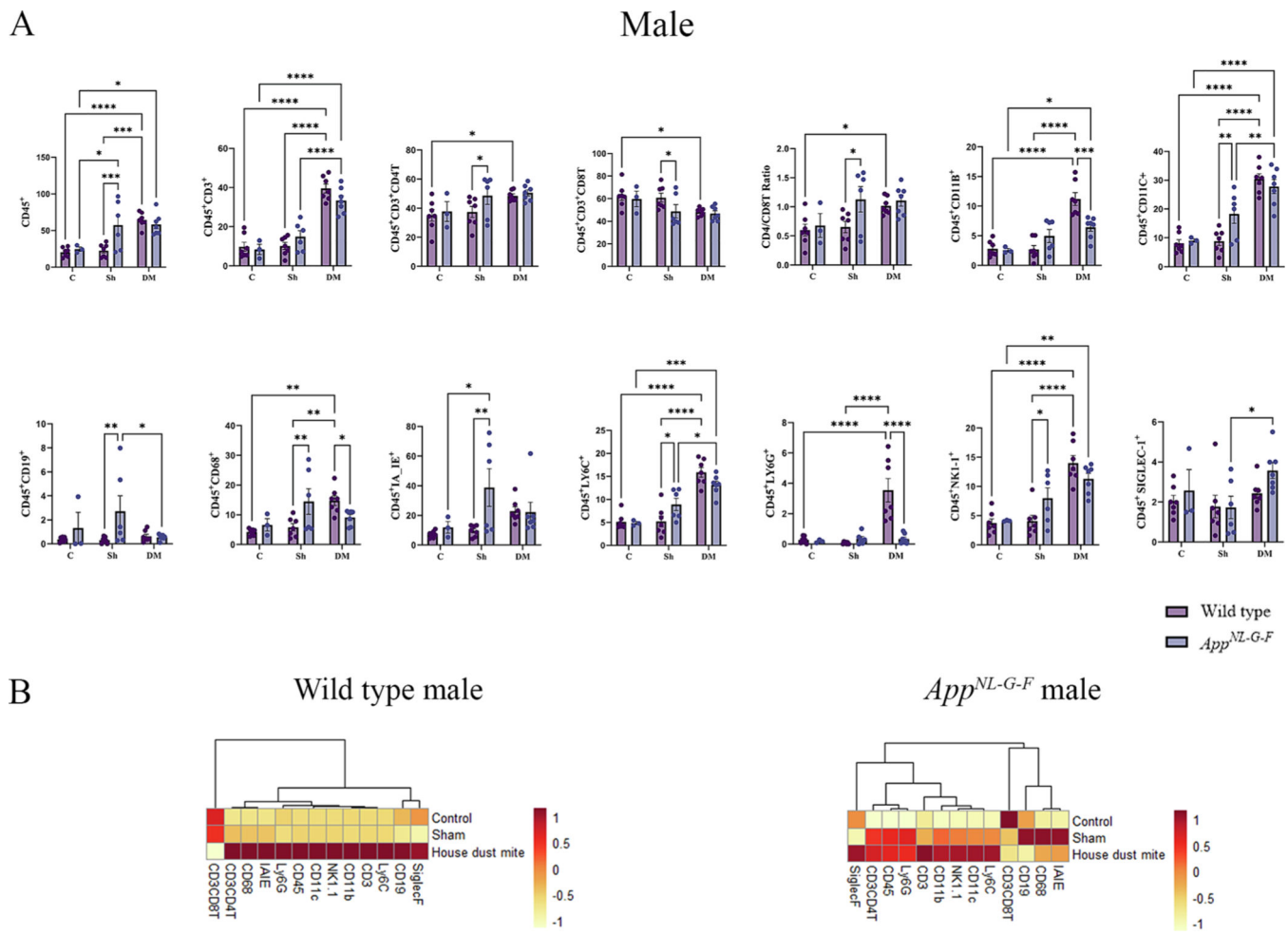

Fig. 1.

House dust mite exposure selectively upregulated specific immune subsets in wild type (WT) and *App*$^{NL\text{-}G\text{-}F}$ male mice. BALF of male WT and *App*$^{NL\text{-}G\text{-}F}$ mice from 16-week exposed control, sham, and HDM exposed (833 μg/kg, 30 min/day, 3 days/week) groups were collected, for flow cytometric analysis for markers of adaptive and innate immune cell phenotypes. (A) Each dot represents data for a single mouse, and bars indicate mean values of % cells (n = 3–9 mice per group) gated through live cells. Results are depicted as mean ± SEM; *p < 0.05, **p < 0.01, ***p < 0.001, and ****p < 0.0001. (B) Column scaled heatmap colors represent the percentage of cells in each subset gated through live cells from a relatively lower percent (in yellow) to a higher percent (in red). Dendrograms indicate the clustering relationships among the groups and % of cell populations, shown above the heatmap. Two-way ANOVAs with interaction between C/Sh/DM (followed by multiple comparisons) and WT/*App*$^{NL\text{-}G\text{-}F}$ produced following statistics; CD45: C/Sh/DM, $F_{2,\ 31} = 15.62$ and $p < 0.0001$, WT/*App*$^{NL\text{-}G\text{-}F}$, $F_{1,31} = 3.740$ and $p = 0.0623$, interaction, $F_{2,\ 31} = 5.638$ and $p = 0.0082$; CD3: C/Sh/DM, $F_{2,\ 31} = 72.86$ and $p < 0.0001$, WT/*App*$^{NL\text{-}G\text{-}F}$, $F_{1,\ 31} = 0.2009$ and $p = 0.6571$, interaction, $F_{2,\ 31} = 2.705$ and $p = 0.0827$; CD4: C/Sh/DM, $F_{2,\ 31} = 4.950$ and $p = 0.0136$, WT/*App*$^{NL\text{-}G\text{-}F}$, $F_{1,\ 31} = 2.502$ and $p = 0.1239$, interaction, $F_{2,\ 31} = 0.8767$ and $p = 0.4262$; CD8: C/Sh/DM, $F_{2,\ 31} = 5.361$ and $p = 0.01$, WT/*App*$^{NL\text{-}G\text{-}F}$,

$F_{1, 31}$ = 2.593 and p = 0.1174, interaction, $F_{2, 31}$ = 1.142 and p = 0.3321; CD4/CD8: C/Sh/DM, $F_{2, 31}$ = 4.780 and p = 0.0155, WT/*App*$^{NL\text{-}G\text{-}F}$, $F_{1,31}$ = 3.977 and p = 0.0550, interaction, $F_{2, 31}$ = 1.571 and p = 0.2239; CD11b: C/Sh/DM, $F_{2, 31}$ = 29.54 and p < 0.0001, WT/*App*$^{NL\text{-}G\text{-}F}$, $F_{1, 31}$ = 1.588 and p = 0.2171, interaction, $F_{2, 31}$ = 9.847 and p = 0.0005; CD11c: C/Sh/DM, $F_{2, 31}$ = 47.42 and p < 0.0001, WT/*App*$^{NL\text{-}G\text{-}F}$, $F_{1, 31}$ = 1.968 and p = 0.1706, interaction, $F_{2, 31}$ = 4.402 and p = 0.0208; CD19: C/Sh/DM, $F_{2, 31}$ = 1.147 and p = 0.2485, WT/*App*$^{NL\text{-}G\text{-}F}$, $F_{1, 31}$ = 4.802 and p = 0.0361, interaction, $F_{2, 31}$ = 2.563 and p = 0.0933; CD68: C/Sh/DM, $F_{2, 31}$ = 4.355 and p = 0.0215, WT/*App*$^{NL\text{-}G\text{-}F}$, $F_{1, 31}$ = 1.046 and p = 0.3143, interaction, $F_{2, 31}$ = 6.651 and p = 0.0039; IA_IE: C/Sh/DM, $F_{2, 31}$ = 2.617 and p = 0.0891, WT/*App*$^{NL\text{-}G\text{-}F}$, $F_{1, 31}$ = 4.371 and p = 0.0449, interaction, $F_{2, 31}$ = 3.458 and p = 0.0441; LY6C: C/Sh/DM, $F_{2, 31}$ = 45.27 and p < 0.0001, WT/*App*$^{NL\text{-}G\text{-}F}$, $F_{1, 31}$ = 0.06460 and p = 0.8010, interaction, $F_{2, 31}$ = 5.291 and p = 0.0105; LY6G: C/Sh/DM, $F_{2, 31}$ = 14.65 and p < 0.0001, WT/*App*$^{NL\text{-}G\text{-}F}$, $F_{1, 31}$ = 9.803 and p = 0.0038, interaction, $F_{2, 31}$ = 13.80 and p < 0.0001; NK1–1: C/Sh/DM, $F_{2, 31}$ = 29.31 and p < 0.0001, WT/*App*$^{NL\text{-}G\text{-}F}$, $F_{1, 31}$ = 0.2934 and p = 0.5919, interaction, $F_{2, 31}$ = 4.369 and p = 0.0213, and SIGLEC-1: C/Sh/DM, $F_{2, 31}$ = 3.893 and p = 0.0310, WT/*App*$^{NL\text{-}G\text{-}F}$, $F_{1, 31}$ = 1.828 and p = 0.1862, interaction, $F_{2, 31}$ = 0.8715 and p = 0.4283.

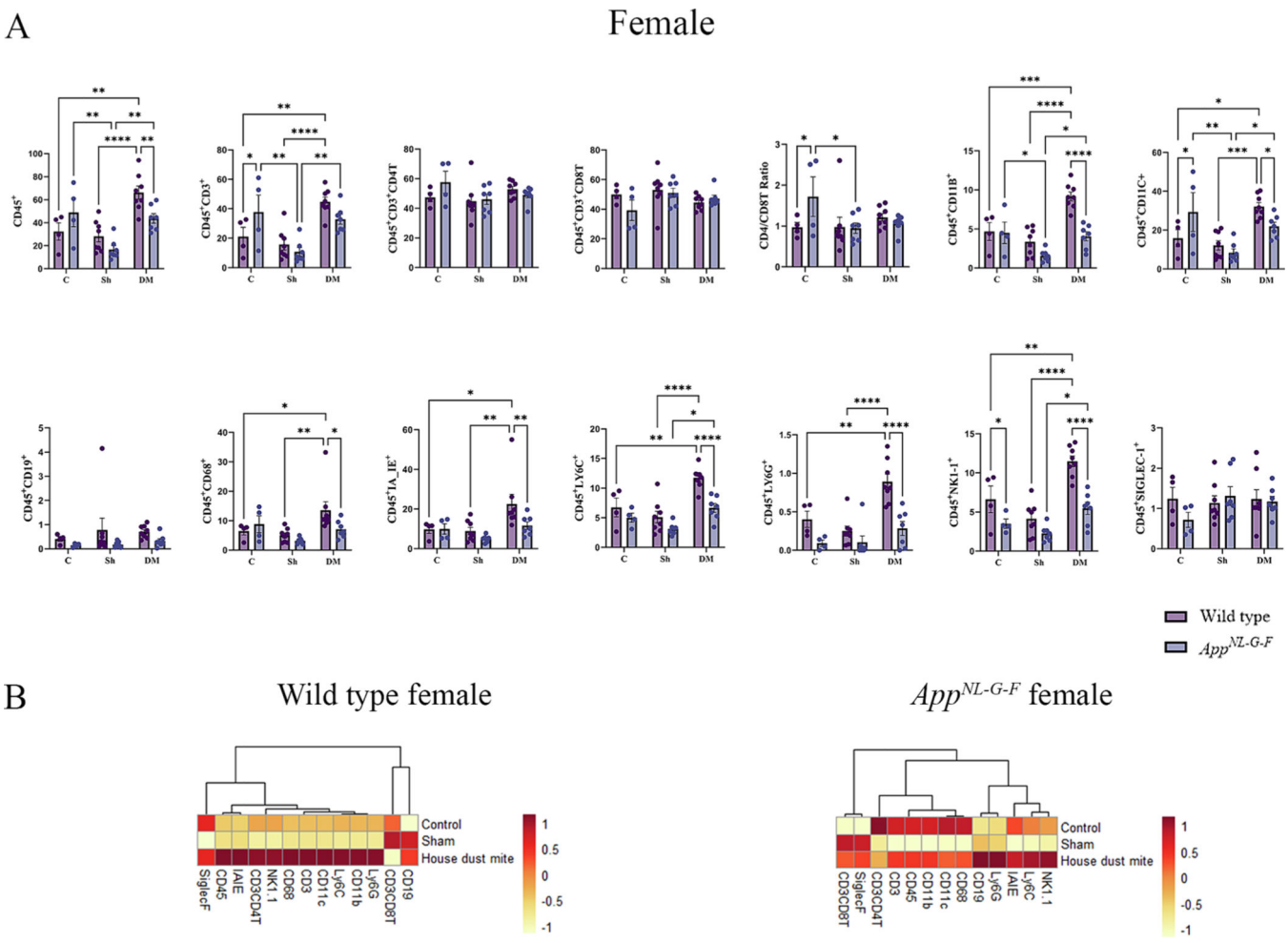

Fig. 2.

House dust mite exposure selectively upregulated specific immune subsets in wild type (WT) and *App*$^{NL\text{-}G\text{-}F}$ female mice. BALF of female WT and *App*$^{NL\text{-}G\text{-}F}$ mice from 16-week exposed control, sham, and HDM exposed (833 μg/kg, 30 min/day, 3 days/week) groups were collected, for flow cytometric analysis for markers of adaptive and innate immune cell phenotypes. (A) Each dot represents data for a single mouse and bars indicate mean values of % positive cells (n = 3–9 mice per group). Results are depicted as mean ± SEM; *p < 0.05, **p < 0.01, ***p < 0.001, and ****p < 0.0001. (B) Column scaled heatmap colors represent the percentage of cells in each subset gated through live cells from a relatively lower percent (in yellow) to a higher percent (in red). Dendrograms indicate the clustering relationships among the groups and % of cell populations, above the heatmap. Two-way ANOVAs with interaction between C/Sh/DM (followed by multiple comparisons) and WT/*App*$^{NL\text{-}G\text{-}F}$ produced following statistics; CD45: C/Sh/DM, $F_{2,\ 32} = 18.55$ and $p < 0.0001$, WT/*App*$^{NL\text{-}G\text{-}F}$, $F_{1,\ 32} = 1.352$ and $p = 0.2535$, interaction, $F_{2,\ 32} = 4.667$ and $p = 0.0166$; CD3: C/Sh/DM, $F_{2,\ 32} = 18.98$ and $p < 0.0001$, WT/*App*$^{NL\text{-}G\text{-}F}$, $F_{1,\ 32} = 0.0002095$ and $p = 0.9885$, interaction, $F_{2,\ 32} = 4.116$ and $p = 0.0257$; CD4: C/Sh/DM, $F_{2,\ 32} = 2.113$ and $p = 0.1374$, WT/*App*$^{NL\text{-}G\text{-}F}$, $F_{1,\ 32} = 0.6920$ and $p = 0.4117$, interaction, $F_{2,\ 32} = 1.524$ and $p = 0.2333$; CD8: C/Sh/DM, $F_{2,\ 32} = 2.556$ and $p = 0.0933$, WT/*App*$^{NL\text{-}G\text{-}F}$, $F_{1,\ 32} = 1.160$ and

p = 0.2895, interaction, $F_{2, 32}$ = 1.483 and p = 0.2421; CD4/CD8: C/Sh/DM, $F_{2, 32}$ = 1.647 and p = 0.2085, WT/*App*$^{NL\text{-}G\text{-}F}$, $F_{1, 32}$ = 1.311 and p = 0.2607, interaction, $F_{2, 32}$ = 2.407 and p = 0.1062; CD11b: C/Sh/DM, $F_{2, 32}$ = 21.55 and p < 0.0001, WT/*App*$^{NL\text{-}G\text{-}F}$, $F_{1, 32}$ = 16.13 and p = 0.0003, interaction, $F_{2, 32}$ = 6.328 and p = 0.0048; CD11c: C/Sh/DM, $F_{2, 32}$ = 14.88 and p < 0.0001, WT/*App*$^{NL\text{-}G\text{-}F}$, $F_{1, 32}$ = 0.003068 and p = 0.9562, interaction, $F_{2, 32}$ = 4.994 and p = 0.0130; CD19: C/Sh/DM, $F_{2, 32}$ = 0.3513 and p = 0.7064, WT/*App*$^{NL\text{-}G\text{-}F}$, $F_{1, 32}$ = 3.385 and p = 0.0751, interaction, $F_{2, 32}$ = 0.1965 and p = 0.8226; CD68: C/Sh/DM, $F_{2, 32}$ = 6.868 and p = 0.0033, WT/*App*$^{NL\text{-}G\text{-}F}$, $F_{1, 32}$ = 1.590 and p = 0.2165, interaction, $F_{2, 32}$ = 2.490 and p = 0.0988; IA_IE: C/Sh/DM, $F_{2, 32}$ = 7.153 and p = 0.0027, WT/*App*$^{NL\text{-}G\text{-}F}$, $F_{1, 32}$ = 3.671 and p = 0.0643, interaction, $F_{2, 32}$ = 1.616 and p = 0.2146; LY6C: C/Sh/DM, $F_{2, 32}$ = 22.09 and p < 0.0001, WT/*App*$^{NL\text{-}G\text{-}F}$, $F_{1, 32}$ = 16.75 and p = 0.0003, interaction, $F_{2, 32}$ = 2.589 and p = 0.0907; LY6G: C/Sh/DM, $F_{2, 32}$ = 13.89 and p < 0.0001, WT/*App*$^{NL\text{-}G\text{-}F}$, $F_{1, 32}$ = 22.09 and p < 0.0001, interaction, $F_{2, 32}$ = 4.065 and p = 0.0267; NK1–1: C/Sh/DM, $F_{2, 32}$ = 26.29 and p < 0.0001, WT/*App*$^{NL\text{-}G\text{-}F}$, $F_{1, 32}$ = 29.11 and p < 0.0001, interaction, $F_{2, 32}$ = 4.111 and p = 0.0258, and SIGLEC-1: C/Sh/DM, $F_{2, 32}$ = 0.6041 and p = 0.5527, WT/*App*$^{NL\text{-}G\text{-}F}$, $F_{1, 32}$ = 0.5909 and p = 0.4477, interaction, $F_{2, 32}$ = 1.115 and p = 0.3402.

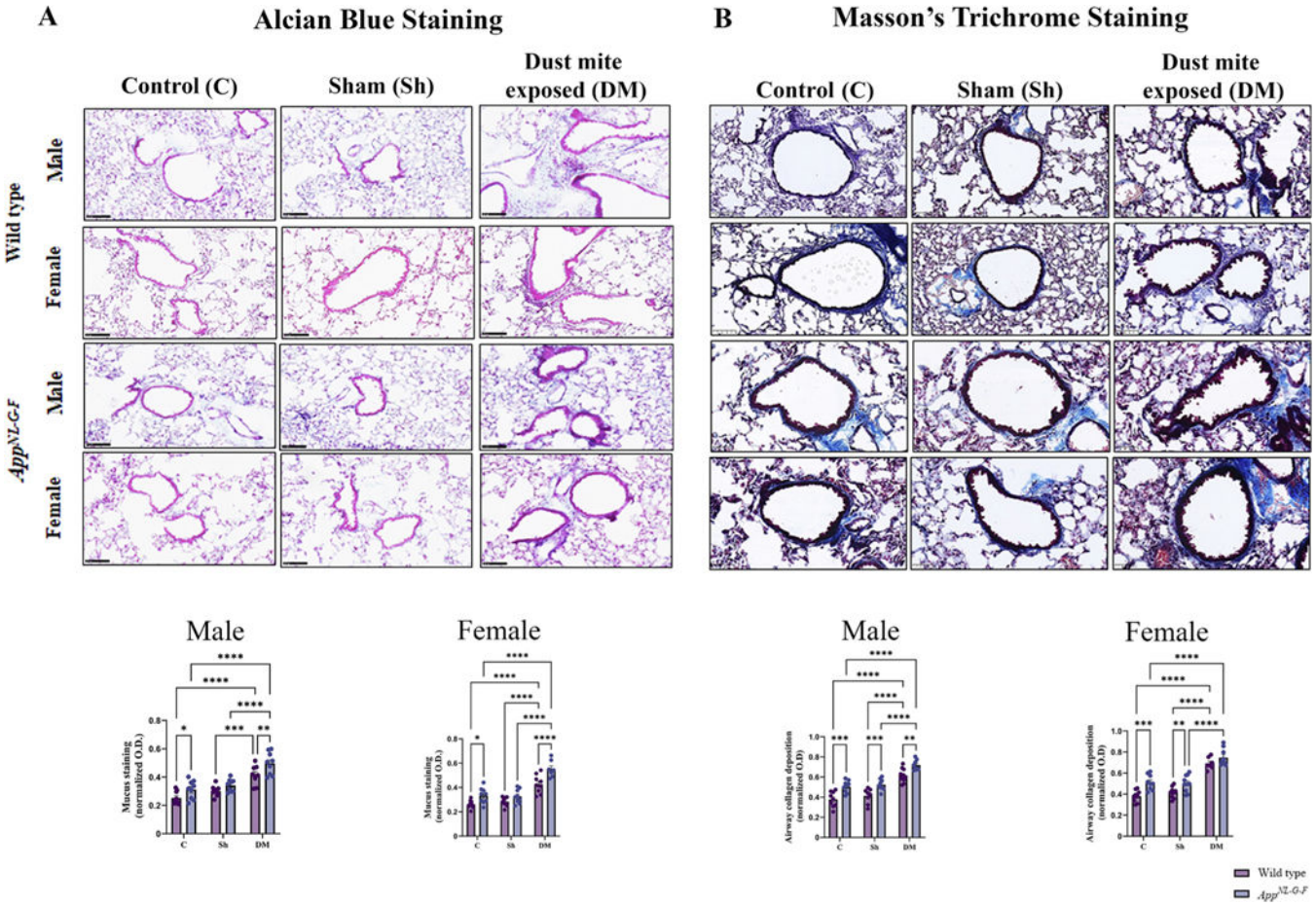

Fig. 3.

House dust mite-exposed lungs displayed increased mucus and collagen production. Lungs of male and female WT and *App*$^{NL\text{-}G\text{-}F}$ mice from 16-week exposed control, sham, and HDM exposed (833 μg/kg, 30 min/day, 3 days/week) groups were collected, sectioned, and stained with Alcian blue (A) and Masson's Trichrome (B) to measure the mucus and collagen production, respectively. Representative immunohistochemical staining images (20x) of the lungs are shown, scale bar 100 μm. Quantification of immunoreactivity was performed, and mucus staining and airway collagen deposition were averaged and graphed. Results are depicted as mean ± SEM; n = 7–10, *p < 0.05, **p < 0.01, ***p < 0.001, and ****p < 0.0001. Two-way ANOVAs with interaction between C/Sh/DM (followed by multiple comparisons) and WT/*App*$^{NL\text{-}G\text{-}F}$ produced following statistics; Alcian blue, male: C/Sh/DM, $F_{2,\ 47} = 42.27$ and p < 0.0001, WT/*App*$^{NL\text{-}G\text{-}F}$, $F_{1,\ 47} = 14.54$ and p = 0.0004, interaction, $F_{2,\ 47} = 0.5611$ and p = 0.5744; Alcian blue, female: C/Sh/DM, $F_{2,\ 46} = 59.54$ and p < 0.0001, WT/*App*$^{NL\text{-}G\text{-}F}$, $F_{1,\ 46} = 25.26$ and p < 0.0001, interaction, $F_{2,\ 46} = 2.241$ and p = 0.1178; Masson's Trichrome, male: C/Sh/DM, $F_{2,\ 47} = 63.77$ and p < 0.0001, WT/*App*$^{NL\text{-}G\text{-}F}$, $F_{1,\ 47} = 40.23$ and p < 0.0001, interaction, $F_{2,\ 47} = 0.1572$ and p = 0.8550, and Masson's Trichrome, female: C/Sh/DM, $F_{2,\ 47} = 85.75$ and p < 0.0001, WT/*App*$^{NL\text{-}G\text{-}F}$, $F_{1,\ 47} = 23.62$ and p < 0.0001, interaction, $F_{2,\ 47} = 1.398$ and p = 0.2572.

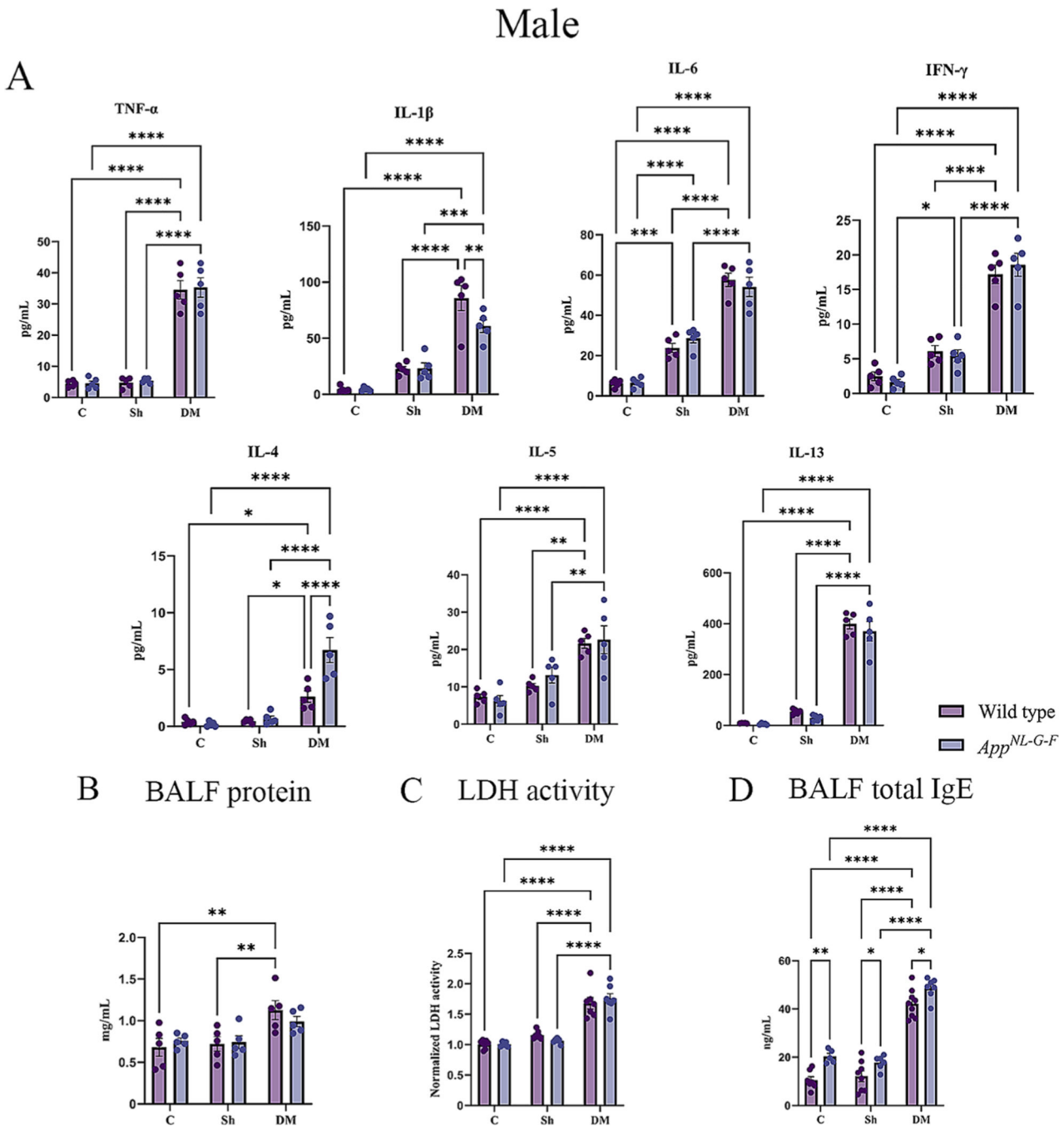

Fig. 4.

House dust mite exposure increased cytokine levels, edema, injury and total IgE in the lungs of wild type (WT) and *App*$^{NL\text{-}G\text{-}F}$ male mice. (A) BALF supernatant of male WT and *App*$^{NL\text{-}G\text{-}F}$ mice from 16-week exposed control, sham, and HDM (833 μg/kg, 30 min/day, 3 days/week) groups, were used for a slide-based mouse cytokine array(A), BALF protein (B) LDH activity (C) and BALF total IgE (D). Results are depicted as mean ± SEM; n = 5, *p < 0.05, **p < 0.01, ***p < 0.001, and ****p < 0.0001. Two-way ANOVAs with interaction between C/Sh/DM (followed by multiple comparisons) and WT/*App*$^{NL\text{-}G\text{-}F}$

produced following statistics; TNF-α: C/Sh/DM, $F_{2, 24}$ = 180.2 and p < 0.0001, WT/*App*$^{NL-G-F}$, $F_{1, 24}$ = 0.1147 and p = 0.7378, interaction, $F_{2, 24}$ = 0.01724 and p = 0.9829; IL-1β: C/Sh/DM, $F_{2, 24}$ = 81.65 and p < 0.0001, WT/*App*$^{NL-G-F}$, $F_{1, 24}$ = 3.193 and p = 0.0866, interaction, $F_{2, 24}$ = 3.148 and p = 0.0494; IL-6: C/Sh/DM, $F_{2, 24}$ = 158.2 and p < 0.0001, WT/*App*$^{NL-G-F}$, $F_{1, 24}$ = 0.06005 and p = 0.8085, interaction, $F_{2, 24}$ = 1.085 and p = 0.3538; IFN-γ: C/Sh/DM, $F_{2, 24}$ = 127.6 and p < 0.0001, WT/*App*$^{NL-G-F}$, $F_{1, 24}$ = 0.002239 and p = 0.9627, interaction, $F_{2, 24}$ = 0.6886 and p = 0.5119; IL-4: C/Sh/DM, $F_{2, 24}$ = 46.84 and p < 0.0001, WT/*App*$^{NL-G-F}$, $F_{1, 24}$ = 10.91 and p = 0.0030, interaction, $F_{2, 24}$ = 11.01 and p = 0.0004; IL-5: C/Sh/DM, $F_{2, 24}$ = 31.74 and p < 0.0001, WT/*App*$^{NL-G-F}$, $F_{1, 24}$ = 0.3287 and p = 0.5718, interaction, $F_{2, 24}$ = 0.5288 and p = 0.5960; IL-13: C/Sh/DM, $F_{2, 24}$ = 272.9 and p < 0.0001, WT/*App*$^{NL-G-F}$, $F_{1, 24}$ = 1.656 and p = 0.2104, interaction, $F_{2, 24}$ = 0.2963 and p = 0.7462; BALF protein: C/Sh/DM, $F_{2, 24}$ = 10.27 and p = 0.0006, WT/*App*$^{NL-G-F}$, $F_{1, 24}$ = 0.03863 and p = 0.8458, interaction, $F_{2, 24}$ = 0.8472 and p = 0.4410; LDH activity: C/Sh/DM, $F_{2, 33}$ = 90.71 and p < 0.0001, WT/*App*$^{NL-G-F}$, $F_{1, 33}$ = 0.01423 and p = 0.9058, interaction, $F_{2, 33}$ = 1.173 and p = 0.3221 and BALF total IgE: C/Sh/DM, $F_{2, 36}$ = 196.4 and p < 0.0001, WT/*App*$^{NL-G-F}$, $F_{1, 36}$ = 23.86 and p < 0.0001, interaction, $F_{2, 36}$ = 0.6668 and p = 0.5196.

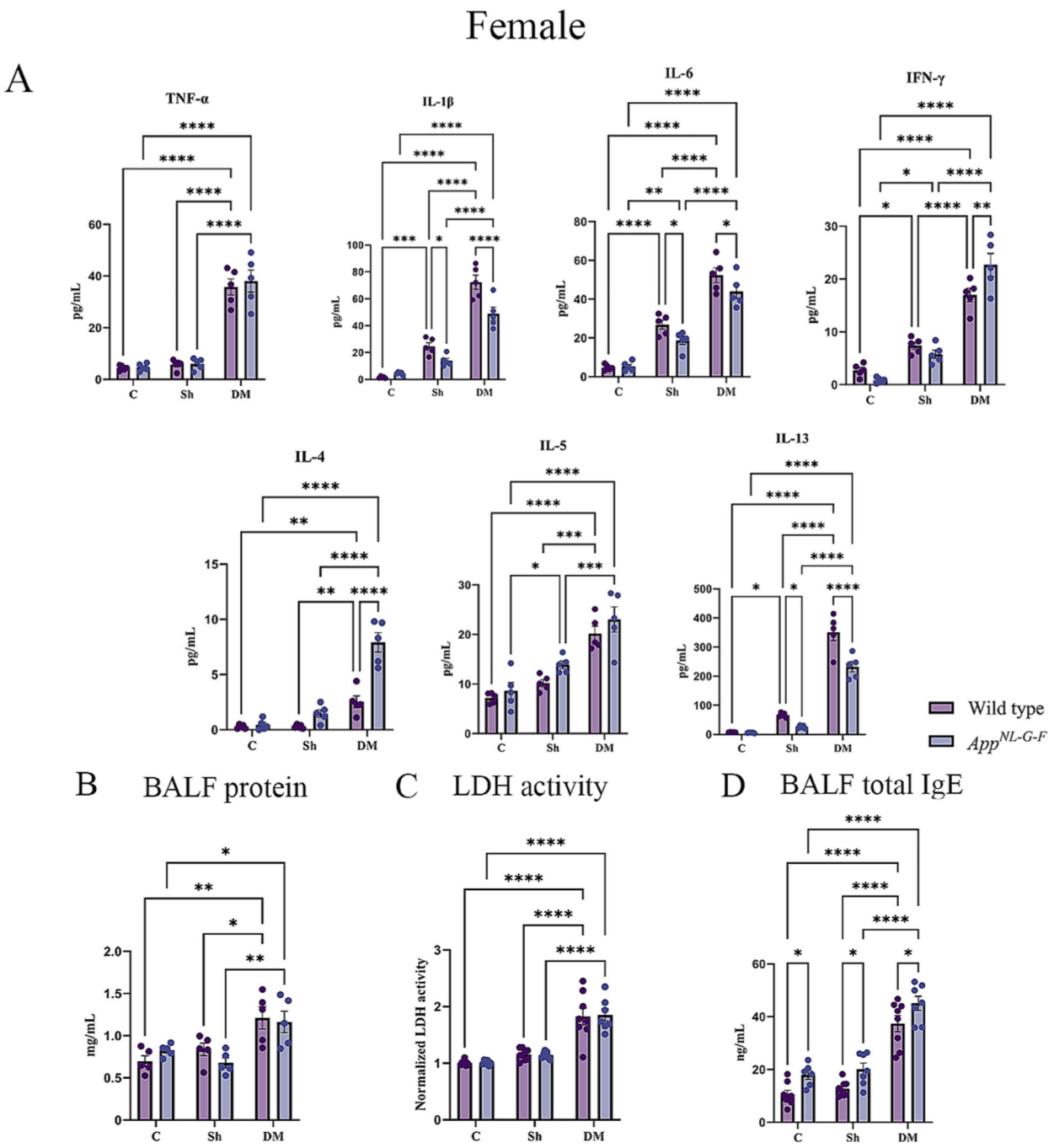

Fig. 5.

House dust mite exposure increased cytokine levels, edema, injury and total IgE in the lungs of wild type (WT) and *App*$^{NL\text{-}G\text{-}F}$ female mice. (A) BALF supernatant of female WT and *App*$^{NL\text{-}G\text{-}F}$ mice from 16-week exposed control, sham, and HDM (833 μg/kg, 30 min/day, 3 days/week) groups, were used for a slide-based mouse cytokine array(A), BALF protein (B) LDH activity (C) and BALF total IgE. Results are depicted as mean ± SEM; n = 5, *p < 0.05, **p < 0.01, ***p < 0.001, and ****p < 0.0001. Two-way ANOVAs with interaction between C/Sh/DM (followed by multiple comparisons) and WT/*App*$^{NL\text{-}G\text{-}F}$

produced following statistics; TNF-α: C/Sh/DM, $F_{2, 24}$ = 133.7 and p < 0.0001, WT/*App*$^{NL-G-F}$, $F_{1, 24}$ = 0.2490 and p = 0.6223, interaction, $F_{2, 24}$ = 0.1355 and p = 0.8740; IL-1β: C/Sh/DM, $F_{2, 24}$ = 166.3 and p < 0.0001, WT/*App*$^{NL-G-F}$, $F_{1, 24}$ = 15.40 and p = 0.0006, interaction, $F_{2, 24}$ = 8.302 and p = 0.0018; IL-6: C/Sh/DM, $F_{2, 24}$ = 142.5 and p < 0.0001, WT/*App*$^{NL-G-F}$, $F_{1, 24}$ = 6.595 and p = 0.0169, interaction, $F_{2, 24}$ = 1.983 and p = 0.1596; IFN-γ: C/Sh/DM, $F_{2, 24}$ = 135.8 and p < 0.0001, WT/*App*$^{NL-G-F}$, $F_{1, 24}$ = 0.6160 and p = 0.4402, interaction, $F_{2, 24}$ = 7.222 and p = 0.0035; IL-4: C/Sh/DM, $F_{2, 24}$ = 70.36 and p < 0.0001, WT/*App*$^{NL-G-F}$, $F_{1, 24}$ = 37.24 and p < 0.0001, interaction, $F_{2, 24}$ = 18.77 and p < 0.0001; IL-5: C/Sh/DM, $F_{2, 24}$ = 46.21 and p < 0.0001, WT/*App*$^{NL-G-F}$, $F_{1, 24}$ = 4.995 and p = 0.0350, interaction, $F_{2, 24}$ = 0.3055 and p = 0.7396; IL-13: C/Sh/DM, $F_{2, 24}$ = 252.6 and p < 0.0001, WT/*App*$^{NL-G-F}$, $F_{1, 24}$ = 22.99 and p < 0.0001, interaction, $F_{2, 24}$ = 9.309 and p = 0.0010; BALF protein: C/Sh/DM, $F_{2, 24}$ = 15.11 and p < 0.0001, WT/*App*$^{NL-G-F}$, $F_{1, 24}$ = 0.1306 and p = 0.7210, interaction, $F_{2, 24}$ = 1.342 and p = 0.2803; LDH activity: C/Sh/DM, $F_{2, 38}$ = 59.70 and p < 0.0001, WT/*App*$^{NL-G-F}$, $F_{1, 38}$ = 0.008313 and p = 0.9278, interaction, $F_{2, 38}$ = 0.02666 and p = 0.9737 and BALF total IgE: C/Sh/DM, $F_{2, 38}$ = 94.47 and p < 0.0001, WT/*App*$^{NL-G-F}$, $F_{1, 38}$ = 17.41 and p = 0.0002, interaction, $F_{2, 38}$ = 0.003438 and p = 0.9966.

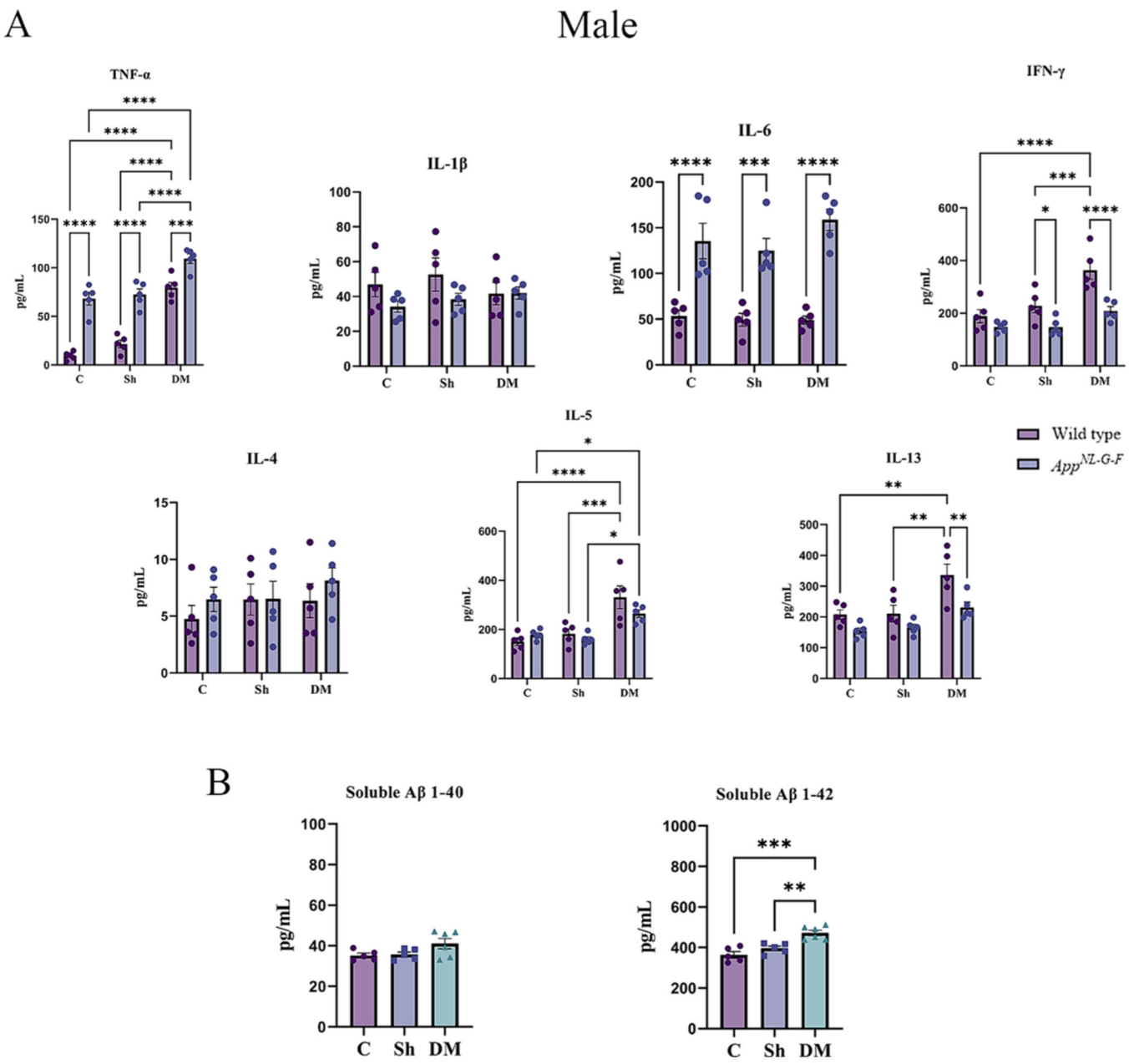

Fig. 6.

House dust mite exposure increased circulating cytokine and soluble Aβ 1–42 levels in wild type (WT) and *App*$^{NL\text{-}G\text{-}F}$ male mice. (A) Serum of male WT and *App*$^{NL\text{-}G\text{-}F}$ mice from 16-week exposed control, sham, and HDM (833 μg/kg, 30 min/day, 3 days/week) groups, were used for a slide-based mouse cytokine array. (B) Serum of male *App*$^{NL\text{-}G\text{-}F}$ mice from control, sham, and house dust mite exposed were used for estimating the levels of soluble Aβ1–40 and 1–42 (B). Results are depicted as mean ± SEM; n = 5–6, *p < 0.05, **p < 0.01, ***p < 0.001, and ****p < 0.0001. Two-way ANOVAs with interaction between C/Sh/DM (followed by multiple comparisons) and WT/*App*$^{NL\text{-}G\text{-}F}$ produced following statistics; TNF-α: C/Sh/DM, $F_{2, 24} = 73.07$ and p < 0.0001, WT/*App*$^{NL\text{-}G\text{-}F}$, $F_{1, 24} = 131.3$ and p < 0.0001, interaction, $F_{2, 24} = 4.526$ and p = 0.0215; IL-1β: C/Sh/DM, $F_{2, 24} = 0.3736$ and p = 0.6922,

WT/*App*$^{NL\text{-}G\text{-}F}$, $F_{1, 24} = 3.305$ and $p = 0.0816$, interaction, $F_{2, 24} = 0.8876$ and $p = 0.4247$; IL-6: C/Sh/DM, $F_{2, 24} = 1.048$ and $p = 0.3663$, WT/*App*$^{NL\text{-}G\text{-}F}$, $F_{1, 24} = 88.45$ and $p < 0.0001$, interaction, $F_{2, 24} = 1.219$ and $p = 0.3132$; IFN-γ: C/Sh/DM, $F_{2, 24} = 15.23$ and $p < 0.0001$, WT/*App*$^{NL\text{-}G\text{-}F}$, $F_{1, 24} = 24.49$ and $p < 0.0001$, interaction, $F_{2, 24} = 3.211$ and $p = 0.0581$; IL-4: C/Sh/DM, $F_{2, 24} = 0.7614$ and $p = 0.4780$, WT/*App*$^{NL\text{-}G\text{-}F}$, $F_{1, 24} = 1.210$ and $p = 0.2823$, interaction, $F_{2, 24} = 0.2725$ and $p = 0.7638$; IL-5: C/Sh/DM, $F_{2, 24} = 21.04$ and $p < 0.0001$, WT/*App*$^{NL\text{-}G\text{-}F}$, $F_{1, 24} = 1.153$ and $p = 0.2937$, interaction, $F_{2, 24} = 2.062$ and $p = 0.1491$ and IL-13: C/Sh/DM, $F_{2, 24} = 13.69$ and $p = 0.0001$, WT/*App*$^{NL\text{-}G\text{-}F}$, $F_{1, 24} = 14.54$ and $p = 0.0008$, interaction, $F_{2, 24} = 1.085$ and $p = 0.3539$. One-way ANOVA multiple comparisons indicate; soluble Aβ 1–40, $F_{2, 13} = 3.027$ and $p = 0.0833$ and soluble Aβ 1–42, $F_{2, 13} = 16.97$ and $p = 0.0002$.

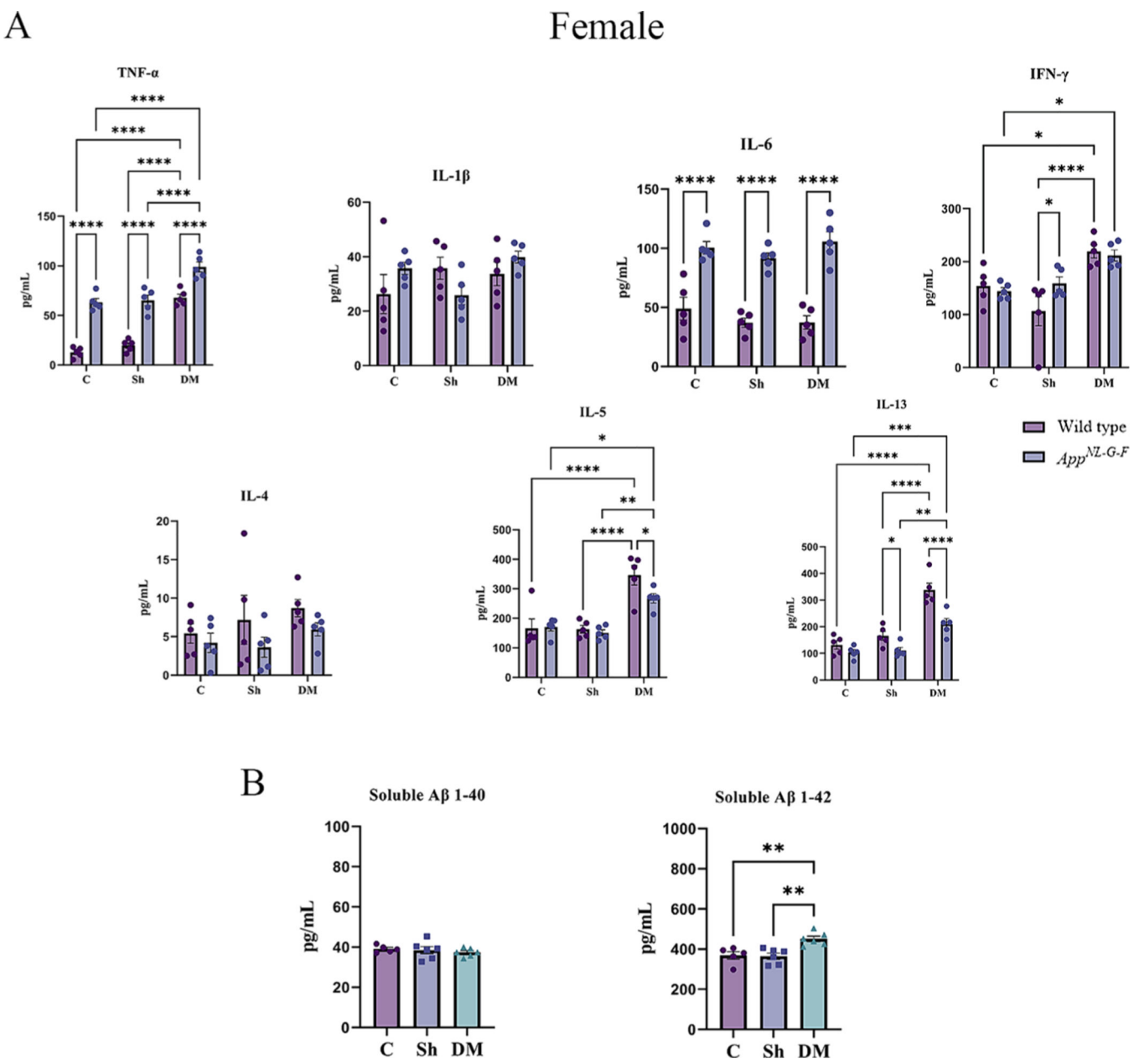

Fig. 7.

House dust mite exposure increased circulating cytokine and soluble Aβ 1–42 levels in wild type (WT) and *App*$^{NL\text{-}G\text{-}F}$ female mice. (A) Serum of female WT and *App*$^{NL\text{-}G\text{-}F}$ mice from 16-week exposed control, sham, and HDM (833 μg/kg, 30 min/day, 3 days/week) groups, were used for a slide-based mouse cytokine array. (B) Serum of female App $^{NL\text{-}G\text{-}F}$ mice from control, sham, and house dust mite exposed were used for estimating the levels of soluble Aβ1–40 and 1–42 (B). Results are depicted as mean ± SEM; n = 5–6, *p < 0.05, **p < 0.01, ***p < 0.001, and ****p < 0.0001. Two-way ANOVAs with interaction between C/Sh/DM (followed by multiple comparisons) and WT/*App*$^{NL\text{-}G\text{-}F}$ produced following statistics; TNF-α: C/Sh/DM, $F_{2, 24} = 80.16$ and p < 0.0001, WT/*App*$^{NL\text{-}G\text{-}F}$, $F_{1, 24} = 172.1$ and p < 0.0001, interaction, $F_{2, 24} = 3.247$ and p = 0.0565; IL-1β: C/Sh/DM, $F_{2, 24} = 1.277$

and p = 0.2970, WT/*App*$^{NL\text{-}G\text{-}F}$, $F_{1, 24}$ = 0.2990 and p = 0.5896, interaction, $F_{2, 24}$ = 2.956 and p = 0.0712; IL-6: C/Sh/DM, $F_{2, 24}$ = 1.316 and p = 0.2869, WT/*App*$^{NL\text{-}G\text{-}F}$, $F_{1, 24}$ = 118.5 and p < 0.0001, interaction, $F_{2, 24}$ = 0.9603 and p = 0.3970; IFN-γ: C/Sh/DM, $F_{2, 24}$ = 15.81 and p < 0.0001, WT/*App*$^{NL\text{-}G\text{-}F}$, $F_{1, 24}$ = 0.8486 and p = 0.3666, interaction, $F_{2, 24}$ = 2.583 and p = 0.0964; IL-4: C/Sh/DM, $F_{2, 24}$ = 1.222 and p = 0.3125, WT/*App*$^{NL\text{-}G\text{-}F}$, $F_{1, 24}$ = 3.360 and p = 0.0792, interaction, $F_{2, 24}$ = 0.2508 and p = 0.7802; IL-5: C/Sh/DM, $F_{2, 24}$ = 29.43 and p < 0.0001, WT/*App*$^{NL\text{-}G\text{-}F}$, $F_{1, 24}$ = 2.600 and p = 0.1200, interaction, $F_{2, 24}$ = 2.050 and p = 0.1507 and IL-13: C/Sh/DM, $F_{2, 24}$ = 47.82 and p < 0.0001, WT/*App*$^{NL\text{-}G\text{-}F}$, $F_{1, 24}$ = 24.46 and p < 0.0001, interaction, $F_{2, 24}$ = 4.420 and p = 0.0232. One-way ANOVA multiple comparisons indicate; soluble Aβ 1–40, $F_{2, 14}$ = 0.4102 and p = 0.6712 and soluble Aβ 1–42, $F_{2, 14}$ = 9.862 and p = 0.0021.

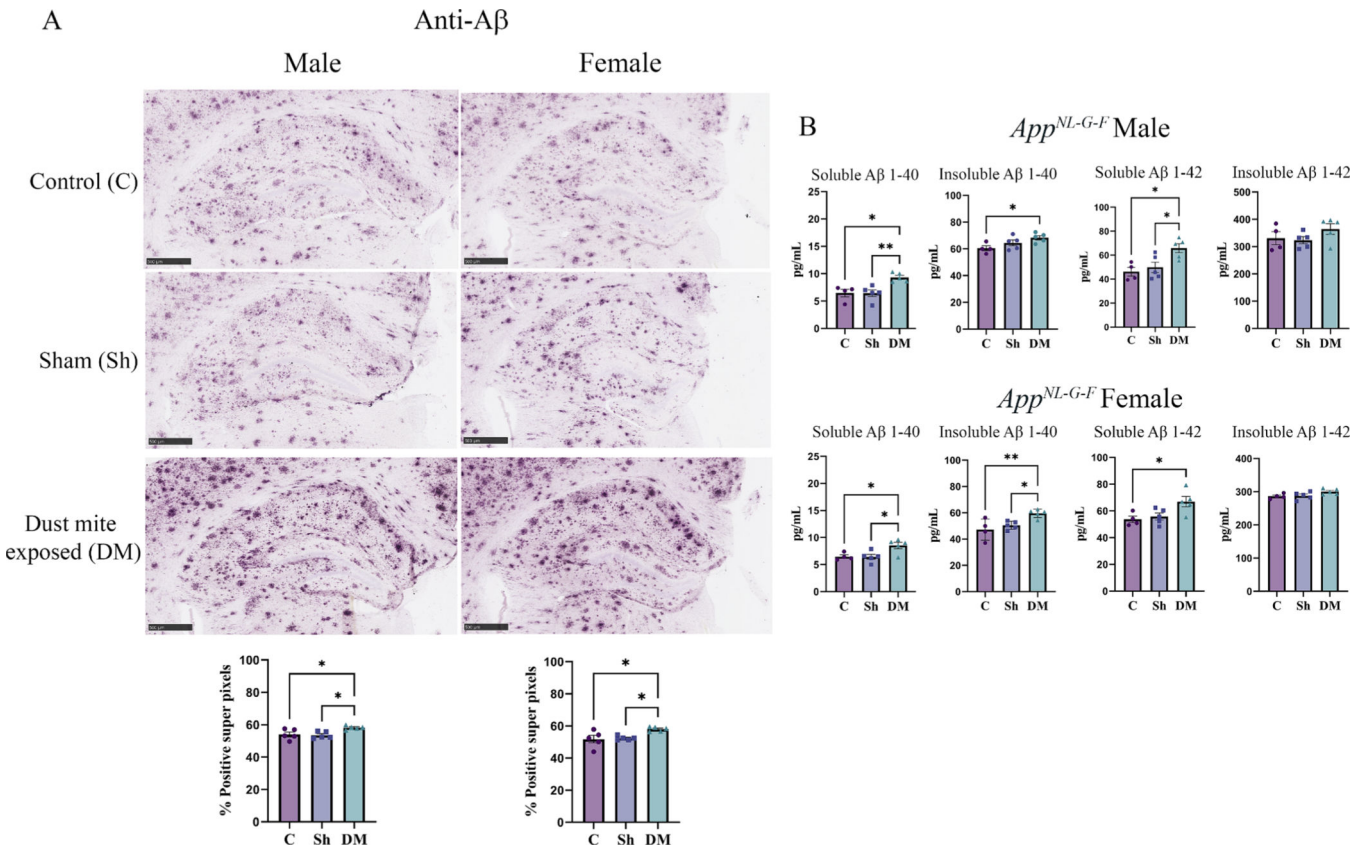

Fig. 8.

House dust mite exposure increased Aβ plaque load. Brains of male and female *App*$^{NL\text{-}G\text{-}F}$ mice from 16-week exposed control, sham, and HDM (833 μg/kg, 30 min/day, 3 days/week) groups were collected, sectioned, and immunostained with anti-Aβ antibody using Vector VIP as the chromogen. (A) Representative immunohistochemical staining images (5x) of the hippocampus are shown, scale bar 500 μm. Quantification of immunoreactivity was performed, and % positive superpixels obtained were averaged and graphed. (B) Both soluble and insoluble Aβ 1–40 and 1–42 were measured from hippocampi of *App*$^{NL\text{-}G\text{-}F}$ mice using ELISAs. Results are depicted as mean ± SEM; n = 5–7, *p < 0.05, **p < 0.01. One-way ANOVA multiple comparisons indicate; $F_{2, 12} = 6.030$ and p = 0.0154 (male, IHC quantification), $F_{2, 12} = 5.860$ and p = 0.0168 (female, IHC quantification), $F_{2, 11} = 9.299$ and p = 0.0043 (male, soluble Aβ 1–40), $F_{2, 11} = 4.061$ and p = 0.0478 (male, insoluble Aβ 1–40), $F_{2, 11} = 6.817$ and p = 0.0119 (male, soluble Aβ 1–42), $F_{2, 11} = 1.445$ and p = 0.2773 (male, insoluble Aβ 1–42), $F_{2, 11} = 6.271$ and p = 0.0152 (female, soluble Aβ 1–40), $F_{2, 11} = 7.574$ and p = 0.0085 (female, insoluble Aβ 1–40), $F_{2, 11} = 5.319$ and p = 0.0242 (female, soluble Aβ 1–42), $F_{2, 11} = 3.161$ and p = 0.0823 (female, insoluble Aβ 1–42).

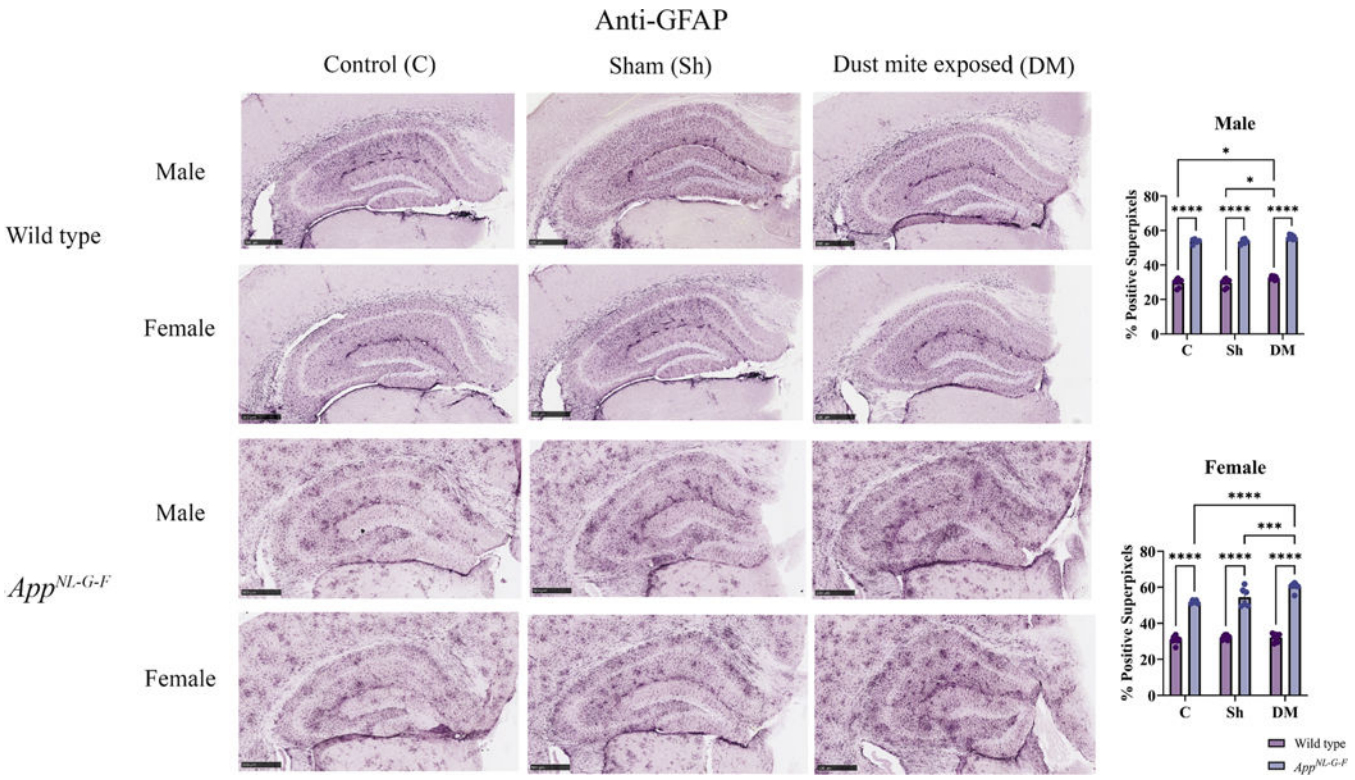

Fig. 9.

House dust mite exposure increased astrogliosis in the hippocampus of *App*$^{NL\text{-}G\text{-}F}$ mice. Brains of male and female WT and *App*$^{NL\text{-}G\text{-}F}$ mice from 16-week exposed control, sham, and HDM exposed (833 μg/kg, 30 min/day, 3 days/week) groups were collected, sectioned, and immunostained with anti-GFAP antibody using Vector VIP as the chromogen. Representative immunohistochemical staining images (5x) of the hippocampus are shown, scale bar 500 μm. Quantification of immunoreactivity was performed, and % positive superpixels obtained were averaged and graphed. Results are depicted as mean ± SEM; n = 5–7, *p < 0.05, ***p < 0.001, and ****p < 0.0001. Two-way ANOVAs with interaction between C/Sh/DM (followed by multiple comparisons) and WT/*App*$^{NL\text{-}G\text{-}F}$ produced following statistics; male: C/Sh/DM, $F_{2, 33} = 8.773$ and $p = 0.0009$, WT/*App*$^{NL\text{-}G\text{-}F}$, $F_{1, 33} = 1557$ and $p < 0.0001$, interaction, $F_{2, 33} = 0.02657$ and $p = 0.9738$ and female: C/Sh/DM, $F_{2, 36} = 11.96$ and $p = 0.0001$, WT/*App*$^{NL\text{-}G\text{-}F}$, $F_{1, 36} = 837.8$ and $p < 0.0001$, interaction, $F_{2, 36} = 7.668$ and $p = 0.0017$.

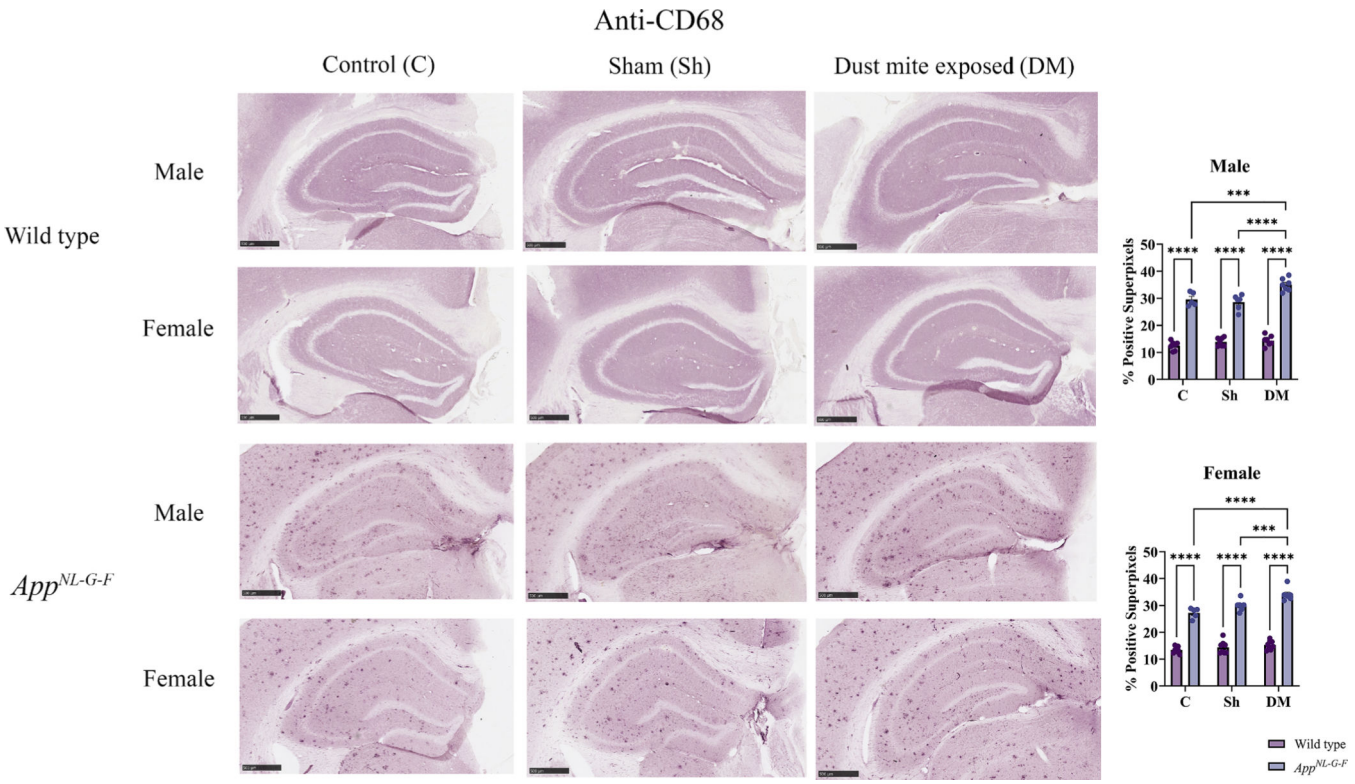

Fig. 10.

House dust mite exposure altered the microglial phenotype marker, CD68, in the hippocampus of *App*$^{NL\text{-}G\text{-}F}$ mice. Brains of male and female WT and *App*$^{NL\text{-}G\text{-}F}$ mice from 16-week exposed control, sham, and HDM (833 μg/kg, 30 min/day, 3 days/week) groups were collected, sectioned, and immunostained with anti-CD68 antibody using Vector VIP as the chromogen. Representative immunohistochemical staining images (5x) of the hippocampus are shown, scale bar 500 μm. Quantification of immunoreactivity was performed, and % positive superpixels obtained were averaged and graphed. Results are depicted as mean ± SEM; n = 5, ***p < 0.001, and ****p < 0.0001. Two-way ANOVAs with interaction between C/Sh/DM (followed by multiple comparisons) and WT/*App*$^{NL\text{-}G\text{-}F}$ produced following statistics; male: C/Sh/DM, $F_{2,\ 33} = 12.43$ and $p < 0.0001$, WT/*App*$^{NL\text{-}G\text{-}F}$, $F_{1,\ 33} = 648.2$ and $p < 0.0001$, interaction, $F_{2,\ 33} = 6.702$ and $p = 0.0036$ and female: C/Sh/DM, $F_{2,\ 37} = 17.74$ and $p < 0.0001$, WT/*App*$^{NL\text{-}G\text{-}F}$, $F_{1,\ 37} = 725.0$ and $p < 0.0001$, interaction, $F_{2,\ 37} = 5.972$ and $p = 0.0057$.

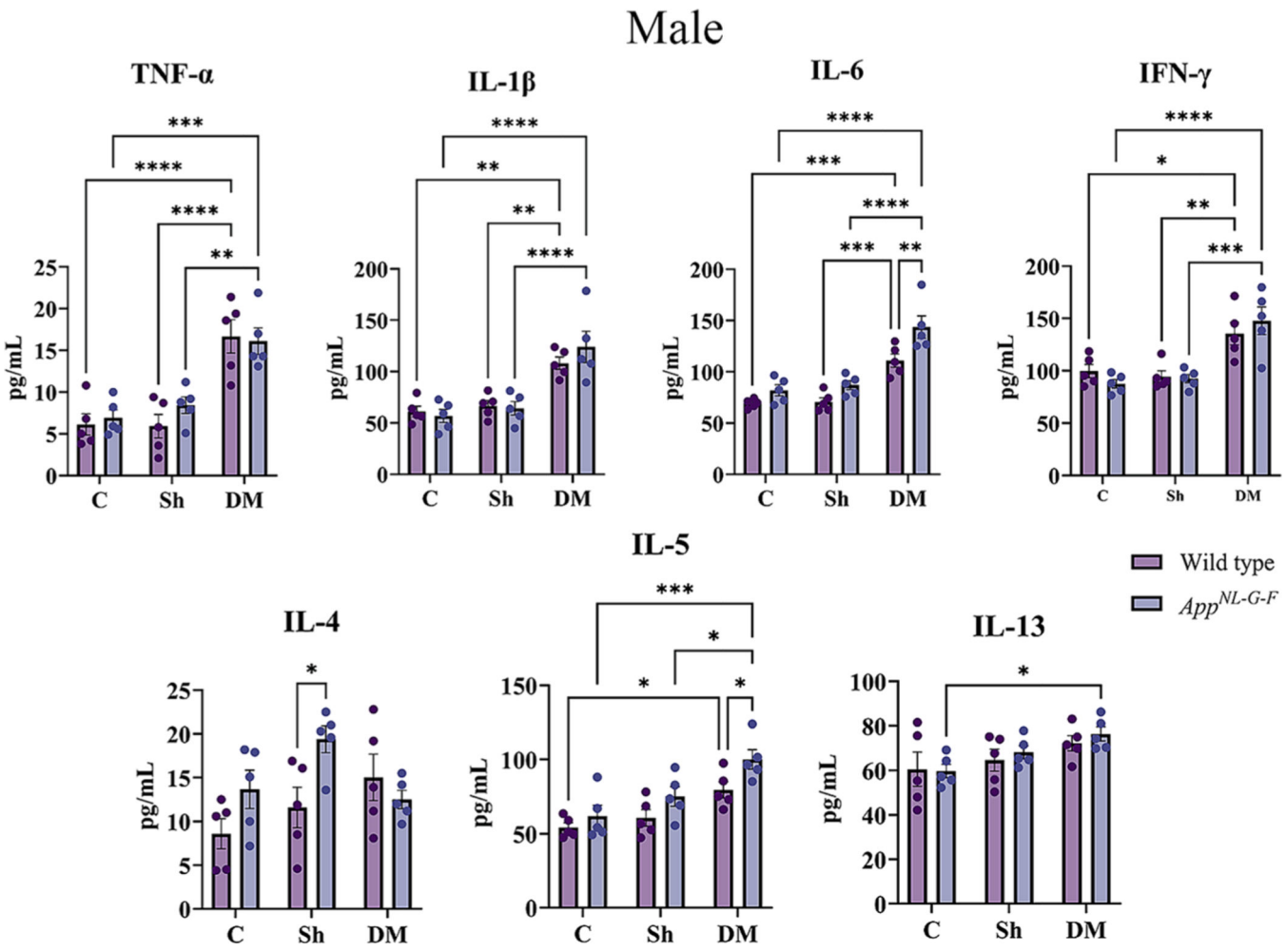

Fig. 11.

House dust mite exposure-induced asthma increased cytokine levels in the brains of wild type (WT) and *App*$^{NL\text{-}G\text{-}F}$ male mice. Temporal cortices of male WT and *App*$^{NL\text{-}G\text{-}F}$ mice from 16-week exposed control, sham, and HDM (833 μg/kg, 30 min/day, 3 days/week) groups, were used for a slide-based mouse cytokine array. Results are depicted as mean ± SEM; n = 5, *p < 0.05, **p < 0.01, ***p < 0.001, and ****p < 0.0001. Two-way ANOVAs with interaction between C/Sh/DM (followed by multiple comparisons) and WT/*App*$^{NL\text{-}G\text{-}F}$ produced following statistics; TNF-α: C/Sh/DM, $F_{2, 24}$ = 30.48 and p < 0.0001, WT/*App*$^{NL\text{-}G\text{-}F}$, $F_{1, 24}$ = 0.6341 and p = 0.4336, interaction, $F_{2, 24}$ = 0.5950 and p = 0.5595; IL-1β: C/Sh/DM, $F_{2, 24}$ = 29.20 and p < 0.0001, WT/*App*$^{NL\text{-}G\text{-}F}$, $F_{1, 24}$ = 0.2201 and p = 0.6432, interaction, $F_{2, 24}$ = 0.9380 and p = 0.4053; IL-6: C/Sh/DM, $F_{2, 24}$ = 43.57 and p < 0.0001, WT/*App*$^{NL\text{-}G\text{-}F}$, $F_{1, 24}$ = 16.53 and p = 0.0004, interaction, $F_{2, 24}$ = 1.433 and p = 0.2583; IFN-γ: C/Sh/DM, $F_{2, 24}$ = 23.37 and p < 0.0001, WT/*App*$^{NL\text{-}G\text{-}F}$, $F_{1, 24}$ = 0.008011 and p = 0.9294, interaction, $F_{2, 24}$ = 1.142 and p = 0.3359; IL-4: C/Sh/DM, $F_{2, 24}$ = 2.451 and p = 0.1075, WT/*App*$^{NL\text{-}G\text{-}F}$, $F_{1, 24}$ = 4.545 and p = 0.0435, interaction, $F_{2, 24}$ = 3.635 and p = 0.0418; IL-5: C/Sh/DM, $F_{2, 24}$ = 15.15 and p < 0.0001, WT/*App*$^{NL\text{-}G\text{-}F}$, $F_{1, 24}$ =

8.808 and p = 0.0067, interaction, $F_{2, 24}$ = 0.5896 and p = 0.5624 and IL-13: C/Sh/DM, $F_{2, 24}$ = 4.877 and p = 0.0167, WT/*App*$^{NL\text{-}G\text{-}F}$, $F_{1, 24}$ = 0.3837 and p = 0.5415, interaction, $F_{2, 24}$ = 0.1787 and p = 0.8375.

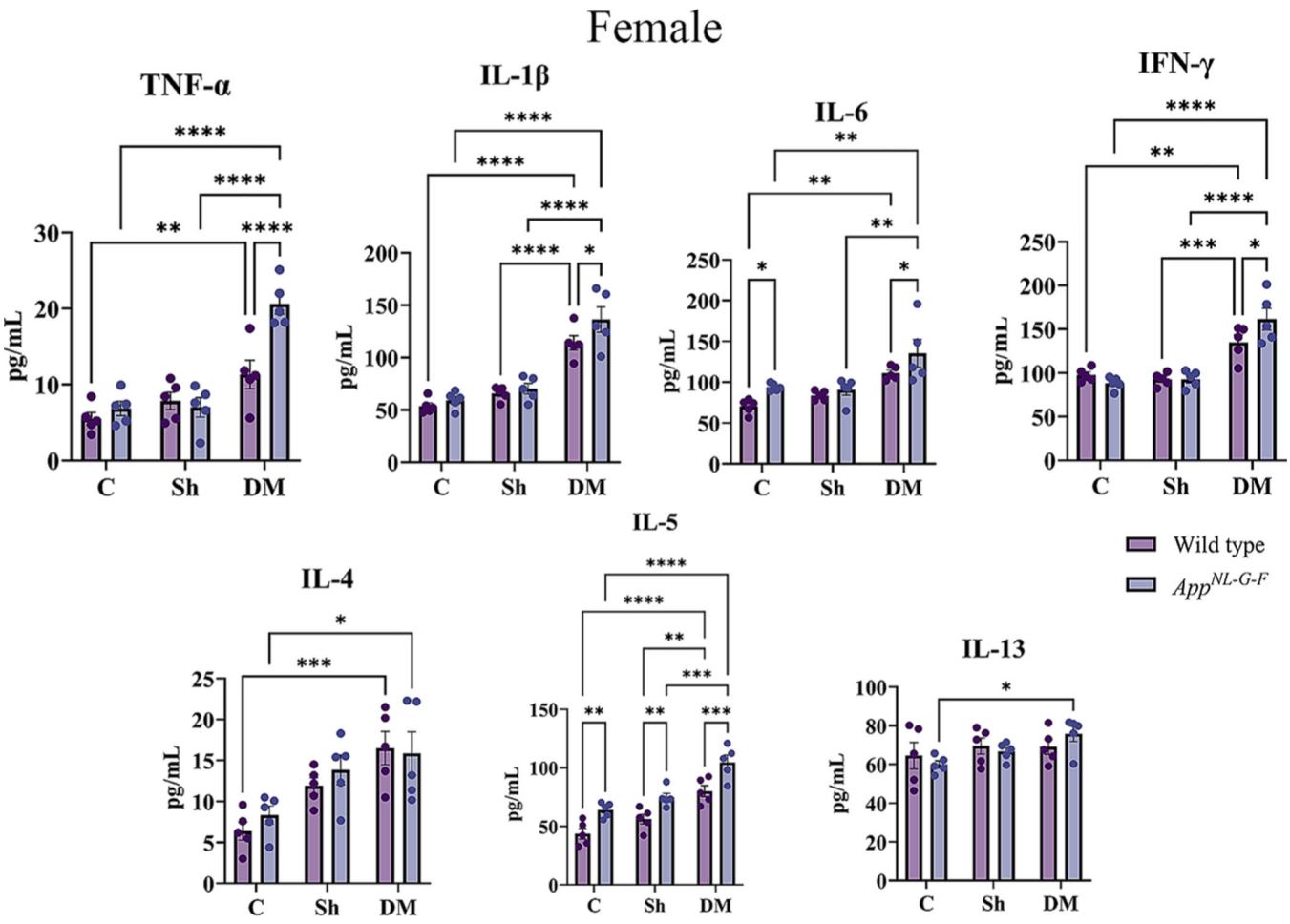

Fig. 12.

House dust mite exposure-induced asthma increased cytokine levels in the brains of wild type (WT) and *App*$^{NL\text{-}G\text{-}F}$ female mice. Temporal cortices of female WT and *App*$^{NL\text{-}G\text{-}F}$ mice from 16-week exposed control, sham, and HDM (833 μg/kg, 30 min/day, 3 days/week) groups, were used for a slide-based mouse cytokine array. Results are depicted as mean ± SEM; n = 5, *p < 0.05, **p < 0.01, ***p < 0.001, and ****p < 0.0001. Two-way ANOVAs with interaction between C/Sh/DM (followed by multiple comparisons) and WT/*App*$^{NL\text{-}G\text{-}F}$ produced following statistics; TNF-α: C/Sh/DM, $F_{2, 24} = 34.79$ and $p < 0.0001$, WT/*App*$^{NL\text{-}G\text{-}F}$, $F_{1, 24} = 9.787$ and $p = 0.0046$, interaction, $F_{2, 24} = 8.613$ and $p = 0.0015$; IL-1β: C/Sh/DM, $F_{2, 24} = 64.55$ and $p < 0.0001$, WT/*App*$^{NL\text{-}G\text{-}F}$, $F_{1, 24} = 4.123$ and $p = 0.0535$, interaction, $F_{2, 24} = 1.205$ and $p = 0.3173$; IL-6: C/Sh/DM, $F_{2, 24} = 16.04$ and $p < 0.0001$, WT/*App*$^{NL\text{-}G\text{-}F}$, $F_{1, 24} = 8.073$ and $p = 0.0090$, interaction, $F_{2, 24} = 0.7745$ and $p = 0.4721$; IFN-γ: C/Sh/DM, $F_{2, 24} = 43.58$ and $p < 0.0001$, WT/*App*$^{NL\text{-}G\text{-}F}$, $F_{1, 24} = 1.097$ and $p = 0.3053$, interaction, $F_{2, 24} = 3.725$ and $p = 0.0390$; IL-4: C/Sh/DM, $F_{2, 24} = 13.36$ and $p = 0.0001$, WT/*App*$^{NL\text{-}G\text{-}F}$, $F_{1, 24} = 0.5964$ and $p = 0.4475$, interaction, $F_{2, 24} = 0.3853$ and $p = 0.6844$; IL-5: C/Sh/DM, $F_{2, 24} = 38.61$ and $p < 0.0001$, WT/*App*$^{NL\text{-}G\text{-}F}$, $F_{1, 24} = 33.32$ and $p < 0.0001$, interaction, $F_{2, 24} = 0.2368$ and $p = 0.7910$ and IL-13: C/Sh/DM, $F_{2, 24} = 3.095$ and $p = 0.0637$, WT/*App*$^{NL\text{-}G\text{-}F}$, $F_{1, 24} = 0.004261$ and $p = 0.9485$, interaction, $F_{2, 24} = 1.097$ and $p = 0.3501$.

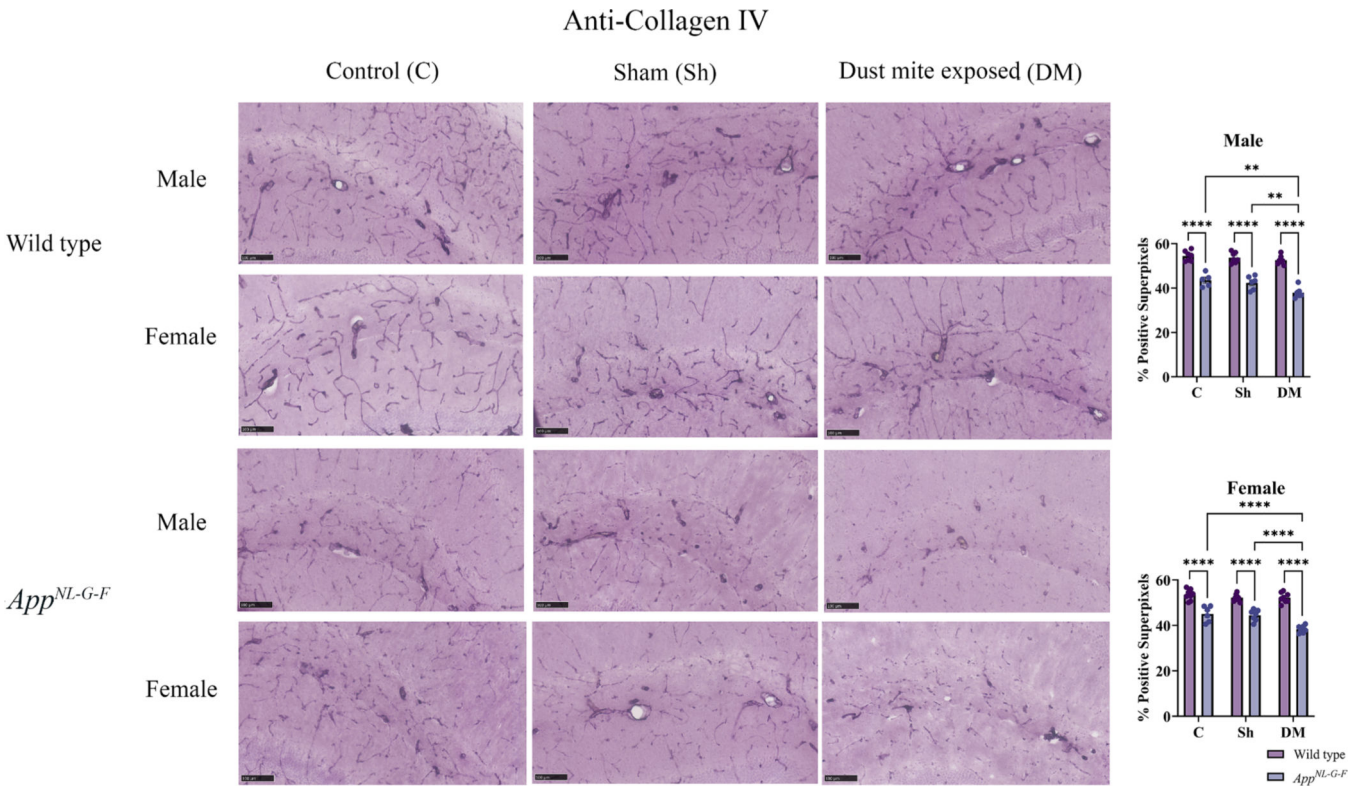

Fig. 13.

House dust mite exposure decreased collagen IV levels in the hippocampus of *App*$^{NL\text{-}G\text{-}F}$. Brains of male and female *App*$^{NL\text{-}G\text{-}F}$ mice from 16-week exposed control, sham, and HDM (833 μg/kg, 30 min/day, 3 days/week) groups were collected, sectioned, and immunostained with anti-collagen IV antibody using Vector VIP as the chromogen. Representative immunohistochemical staining images (5x) of the hippocampus are shown, scale bar 100 μm. Quantification of immunoreactivity was performed, and % positive superpixels obtained were averaged and graphed. Results are depicted as mean ± SEM; n = 5–7, **p < 0.01 and ****p < 0.0001. Two-way ANOVAs with interaction between C/Sh/DM (followed by multiple comparisons) and WT/*App*$^{NL\text{-}G\text{-}F}$ produced following statistics; male: C/Sh/DM, $F_{2, 33} = 8.134$ and $p = 0.0013$, WT/*App*$^{NL\text{-}G\text{-}F}$, $F_{1, 33} = 231.7$ and $p < 0.0001$, interaction, $F_{2, 33} = 2.379$ and $p = 0.1084$ and female: C/Sh/DM, $F_{2, 38} = 12.10$ and $p < 0.0001$, WT/*App*$^{NL\text{-}G\text{-}F}$, $F_{1, 38} = 206.0$ and $p < 0.0001$, interaction, $F_{2, 38} = 7.783$ and $p = 0.0015$.